Asymmetric inertial instability

V. Zeitlin

[1]Institut Universitaire de France

[2]Laboratory of Dynamical Meteorology, University P. and M. Curie, Paris, France

UCL, December 2013

Instabilities of jets in stratified rotating fluids

Instabilities known/expected for jets in stratified rotating fluid:

- short-wave Kelvin-Helmholtz (KH) instability for strong vertical shears
- long-wave barotropic instability (*BTI*)
- long-wave baroclinic instability (*BCI*)
- symmetric inertial instability (*II*)

Interpretation of instabilities:

Phase-locking and resonance of the linear waves (counter)propagating in the background flow $\rightarrow$ instability.
Possible types of propagating waves:

- Poincaré (P) or inertia-gravity
- Baroclinic and barotropic Rossby (R)

Physical origin: "elasticity" of the iso-density surfaces (P), "elasticity" of the iso-PV surfaces (R).

Remark:

Equatorial waves - extra types: Kelvin and Yanai (mixed inertia-gravity) waves.

Wave origins of jet instabilities

"Standard" instabilities

- *KH*: P-P resonance
- *BTI*: barotropic R - R resonance (standard: geostrophic)
- *BCI*: baroclinic R - R resonance (standard: geostrophic)

"Non-standard" inertial instability (*II*)

Trapped waves with negative eigen square frequency.

- essentially ageostrophic: needs $Ro = \mathcal{O}(1)$;
- symmetric with resp. to along-jet translations;
- needs vertical variations.

Motivations

Questions

- How along-jet modulations influence *II*?
- What is the relation of *II* to *BCI* and *BTI*?
- What is essentially ageostrophic *BCI*?
- How *II* saturates nonlinearly and what is the difference with the *BCI*/*BTI* saturation?
- *II* is endemic on the equator - differences between mid-latitude and equatorial *II*?

The strategy and techniques

The strategy

- Detailed linear stability analysis in a wide range of *Ro*
- High resolution NS of the saturation initialized with the most unstable eigenmodes

Models

2-layer Rotating Shallow Water, f- and equatorial β-plane; Primitive Equations

The method

- stability analysis: pseudospectral collocation
- NS: finite-volume well-balanced for RSW, WRF for PE

2-layer RSW model on the f-plane

$$\begin{cases} (\partial_t + u_1\partial_x + v_1\partial_y)u_1 - fv_1 + g\partial_x(h_1 + h_2) = 0, \\ (\partial_t + u_1\partial_x + v_1\partial_y)v_1 + fu_1 + g\partial_y(h_1 + h_2) = 0, \\ \partial_t h_1 + \partial_x(h_1u_1) + \partial_y(h_1v_1) = 0, \\ (\partial_t + u_2\partial_x + v_2\partial_y)u_2 - fv_2 + g\partial_x(rh_1 + h_2) = 0, \\ (\partial_t + u_2\partial_x + v_2\partial_y)v_2 + fu_2 + g\partial_y(rh_1 + h_2) = 0, \\ \partial_t h_2 + \partial_x(h_2u_2) + \partial_y(h_2v_2) = 0. \end{cases} \quad (2.1)$$

u_i, v_i $i = 1, 2$ are x and y components of the velocity in layer i (layer 1 on top of the layer 2), h_i are the thicknesses of the layers, $r = \frac{\rho_1}{\rho_2} \leq 1$, $f = const$ is the Coriolis parameter, and g is gravity.

Barotropic Bickley jet I

$$\begin{cases} h_1 = H_1(x) = H_{10} \\ h_2 = H_2(x) = H_{20} + \delta \tanh\left(\frac{x}{L}\right) \end{cases} \quad \begin{cases} U_1(x) = U_2(x) = 0 \\ V_{1,2}(x) = V(x) = \\ \frac{g\delta}{fL}\left(1 - \tanh^2\left(\frac{x}{L}\right)\right) \end{cases} \quad (2.2)$$

H_{10}, $H_{20} = const$, L and δ - width and intensity of the jet, $V_0 = \frac{g\delta}{fL}$ - peak velocity. Dimensionless parameters: $Bu = \frac{gH_0}{f^2L^2}$, $Ro = \frac{g\delta}{(fL)^2}$, $d = \frac{H_{20}}{H_{10}}$, r, $H_0 = H_{10} + H_{20}$.

Barotropic Bickley jet II

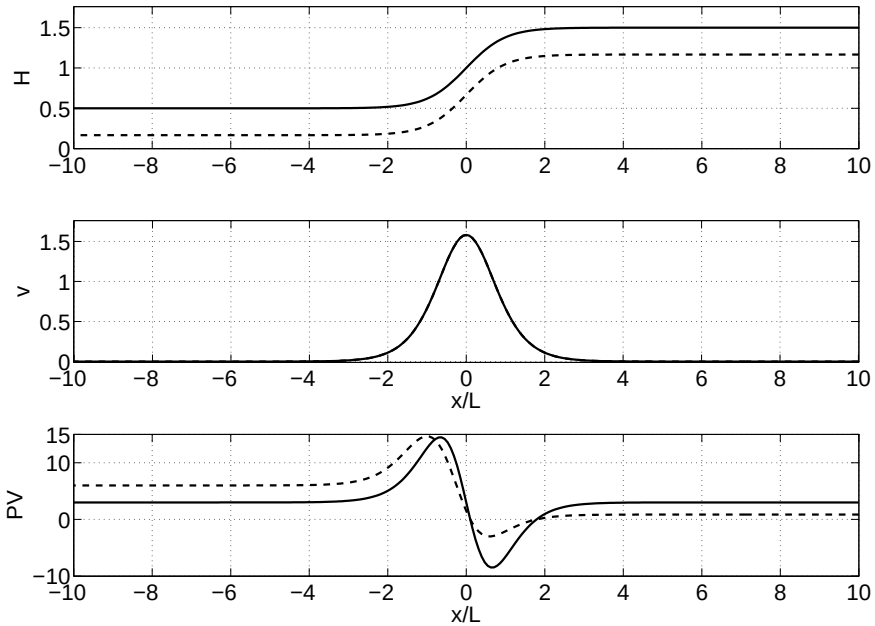

Background jet profile as a function of x/L for $\frac{\delta}{L} = \sqrt{\frac{5}{2}}$; solid: layer 1; dashed: layer 2.

Linearization of the symmetric problem

Small perturbations of the jet (2.2):

$$h_i = H_i(x)+\eta_i'(x,t),\ u_i = u_i'(x,t),\ v_i = V(x)+v_i'(x,t), \qquad i = 1,2, \tag{2.3}$$

Solution is sought in the form
$(u_i', v_i', \eta_i') = (u_{0i}(x), v_{0i}(x), \eta_{0i}(x))\, e^{-i\omega t} + \text{c.c.} \rightarrow$ a pair of coupled Schrödinger equations for the across-front velocities of the layers:

$$\left(-\omega^2 + f(f+\partial_x V)\right)\begin{pmatrix} u_{01} \\ u_{02} \end{pmatrix} - g\partial_x^2 \begin{pmatrix} H_1 u_{01} + H_2 u_{02} \\ rH_1 u_{01} + H_2 u_{02} \end{pmatrix} = 0. \tag{2.4}$$

Eigenfrequencies

In terms of the barotropic and the baroclinic velocity components:

$$\begin{pmatrix} u_b \\ u_B \end{pmatrix} = \begin{pmatrix} u_{02} - u_{01} \\ \frac{H_1 u_{01} + H_2 u_{02}}{H_1 + H_2} \end{pmatrix}. \tag{2.5}$$

$$\begin{aligned} \omega^2 &= f \frac{\int (f + \partial_x V) H_b |u_b|^2}{\int H_b |u_b|^2} + g(1-r) \frac{\int |\partial_x (H_b u_b)|^2}{\int H_b |u_b|^2} \\ &+ g(1-r) \frac{\int H_b u_b^* \partial_x^2 (H_1 u_B)}{\int H_b |u_b|^2}, \end{aligned} \tag{2.6}$$

where $H_b = \frac{1}{1/H_1 + 1/H_2}$.

Relative vorticity of the jet $\partial_x V$ sufficiently negative $\Rightarrow \omega^2 < 0$

$\Rightarrow$ inertial (symmetric) instability.

A typical unstable mode for $Bu = 10, Ro = 5, d = 2, r = 0.5$

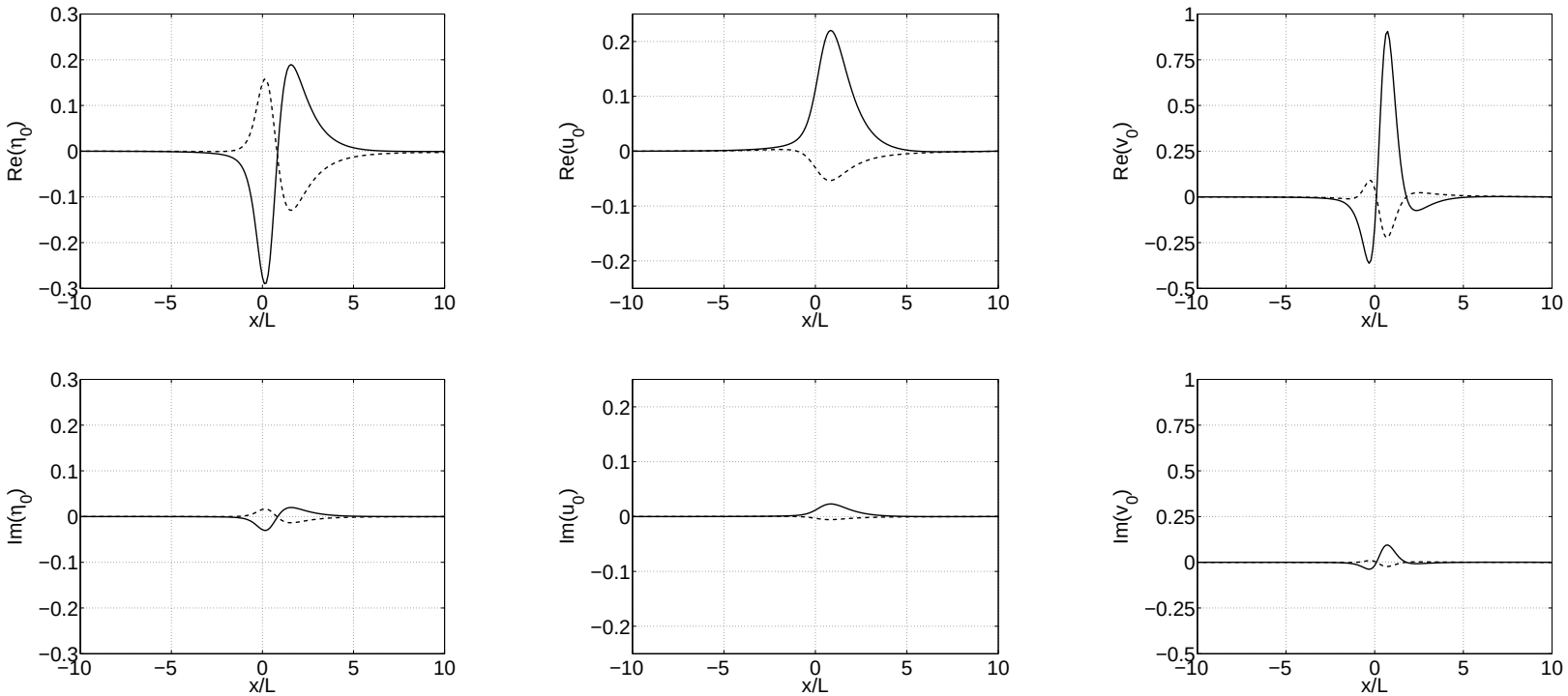

Stability diagram for small *Ro*

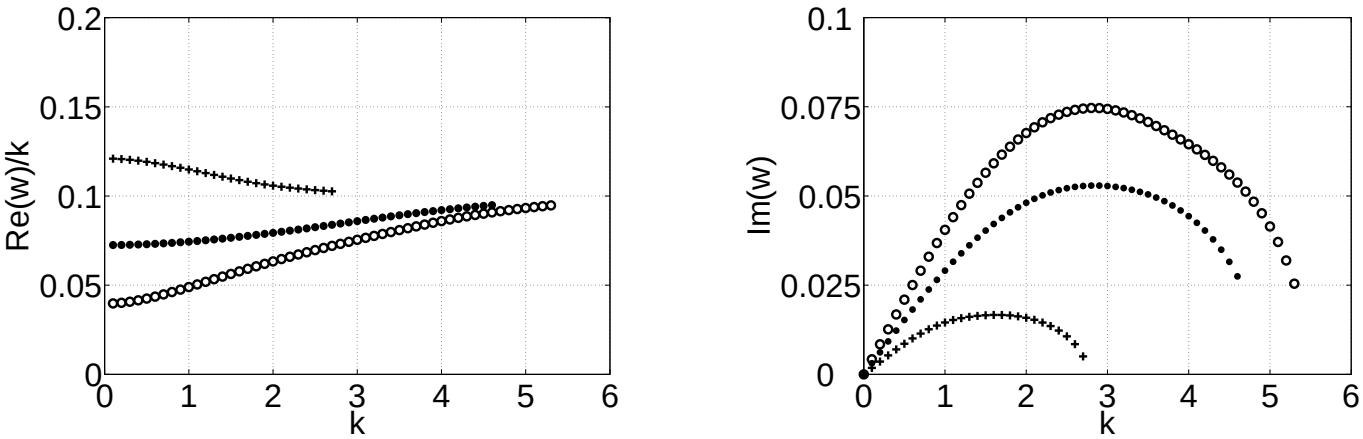

Left: phase speed $Re(\omega)/k$ as a function of k; *Right:* Growth rate $Im(\omega)$ as a function of k. Quasi-geostrophic jet: $H_0 = 1, Bu = 10, Ro = 0.5, d = 2, r = 0.5$.

Cross-section of the most unstable mode

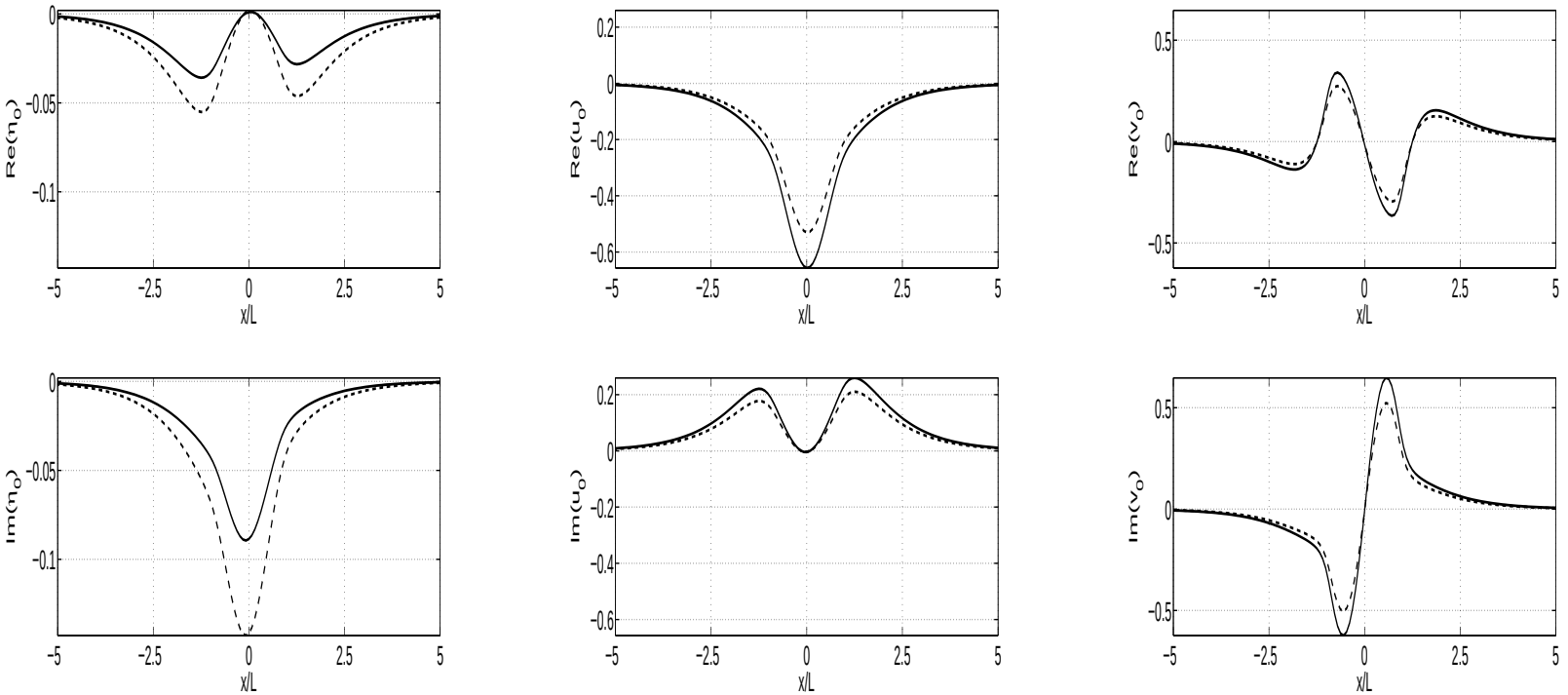

Solid (dashed): layer 1 (2) $\Rightarrow$ barotropic instability

2D structure of the most unstable mode

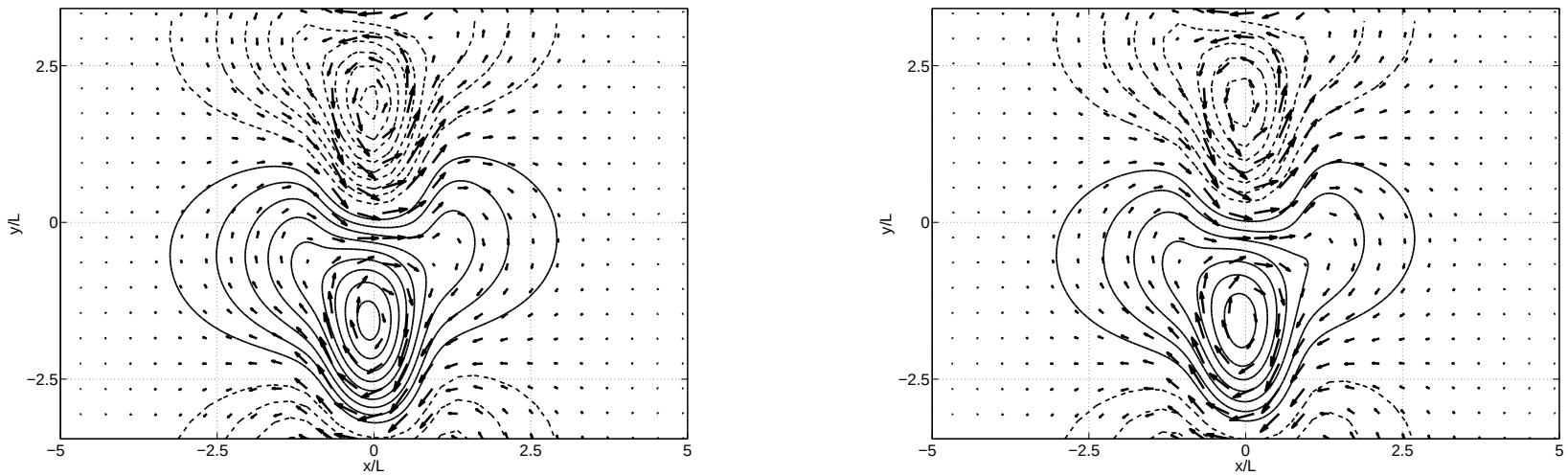

Left(Right): upper(lower) layer $\Rightarrow$ barotropic instability.

Cross-section of the second-unstable mode

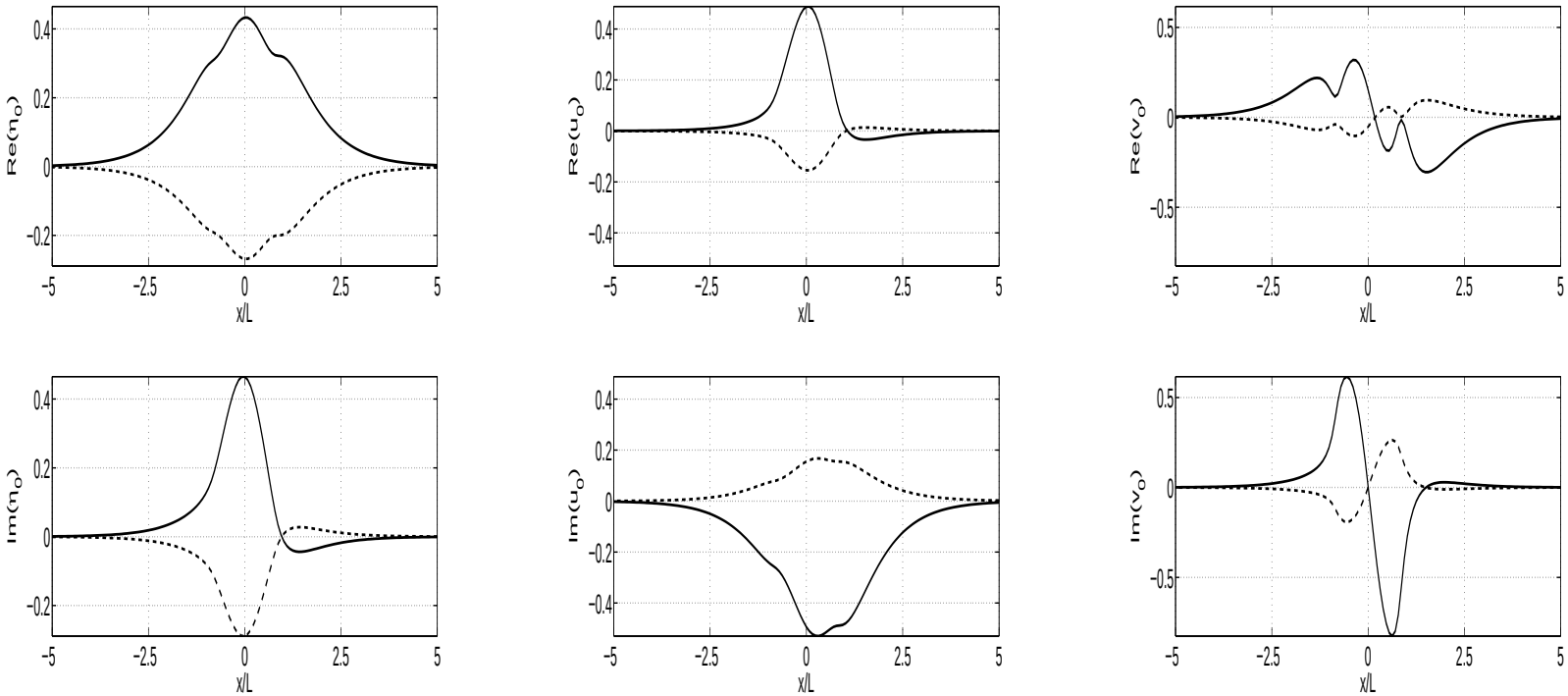

Solid (dashed): layer 1 (2) $\Rightarrow$ baroclinic instability

2D structure of the second - unstable mode

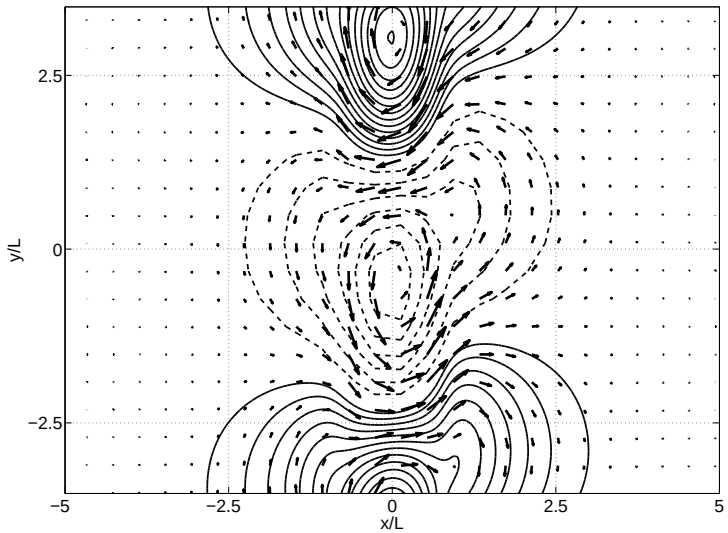

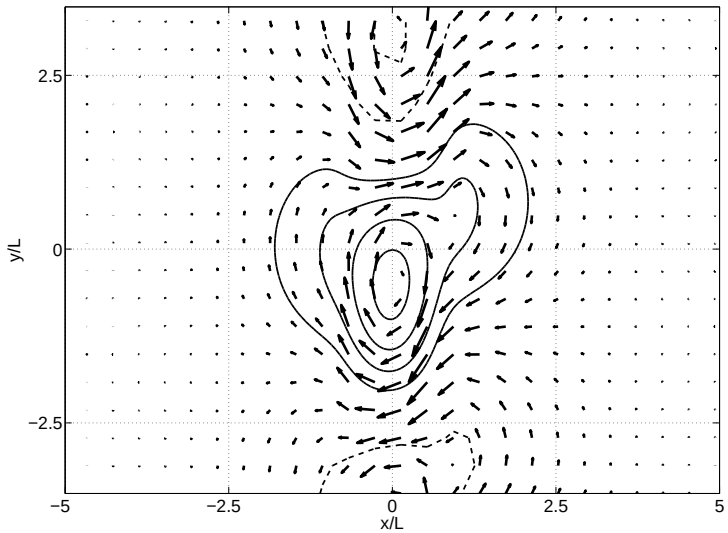

Motion in the layers is quite opposite $\rightarrow$ monopolar baroclinic

2D structure of the third-unstable mode

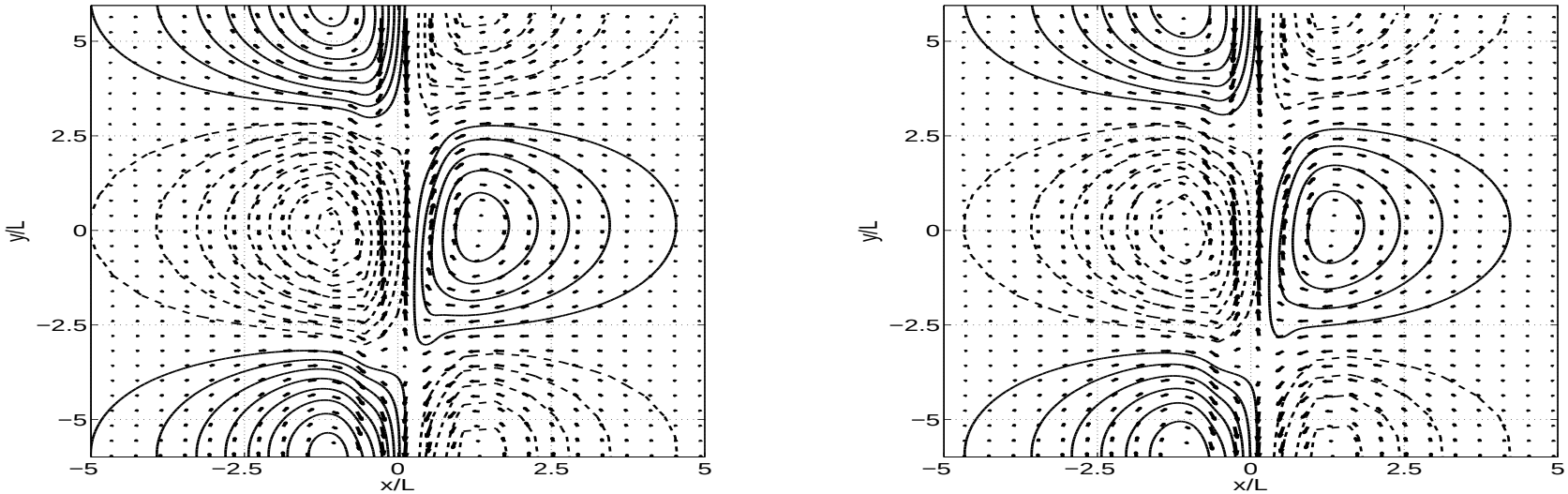

Dipolar barotropic mode.

Stability diagram for large *Ro*

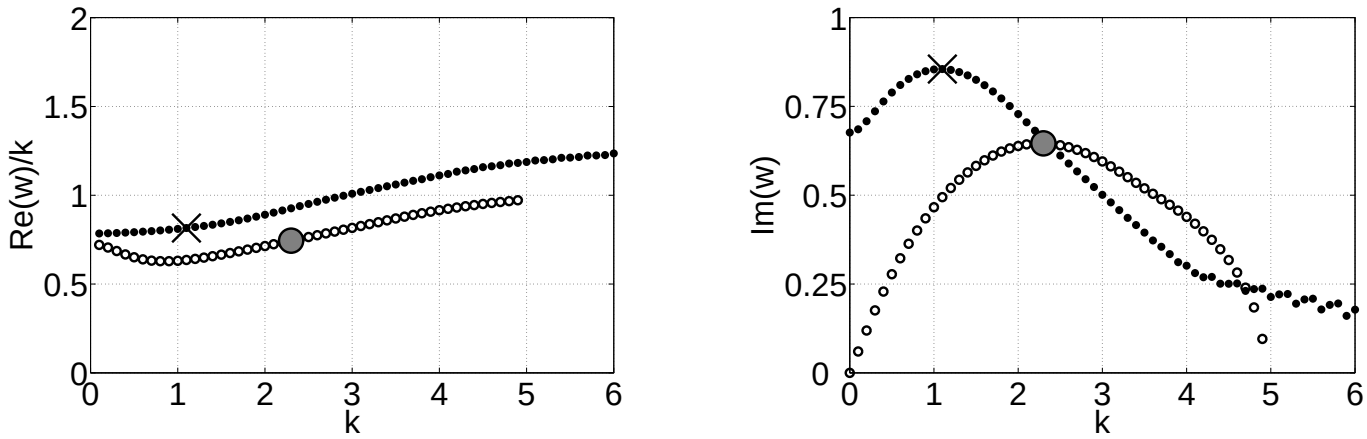

Left: phase speed $Re(\omega)/k$ as a function of k; *Right:* Growth rate $Im(\omega)$ as a function of k. Strongly ageostrophic jet: $H_0 = 1, Bu = 10, Ro = 5, d = 2, r = 0.5$. BCI growth rate has non-zero limit at $k \to 0$.

Cross-section of the most unstable mode

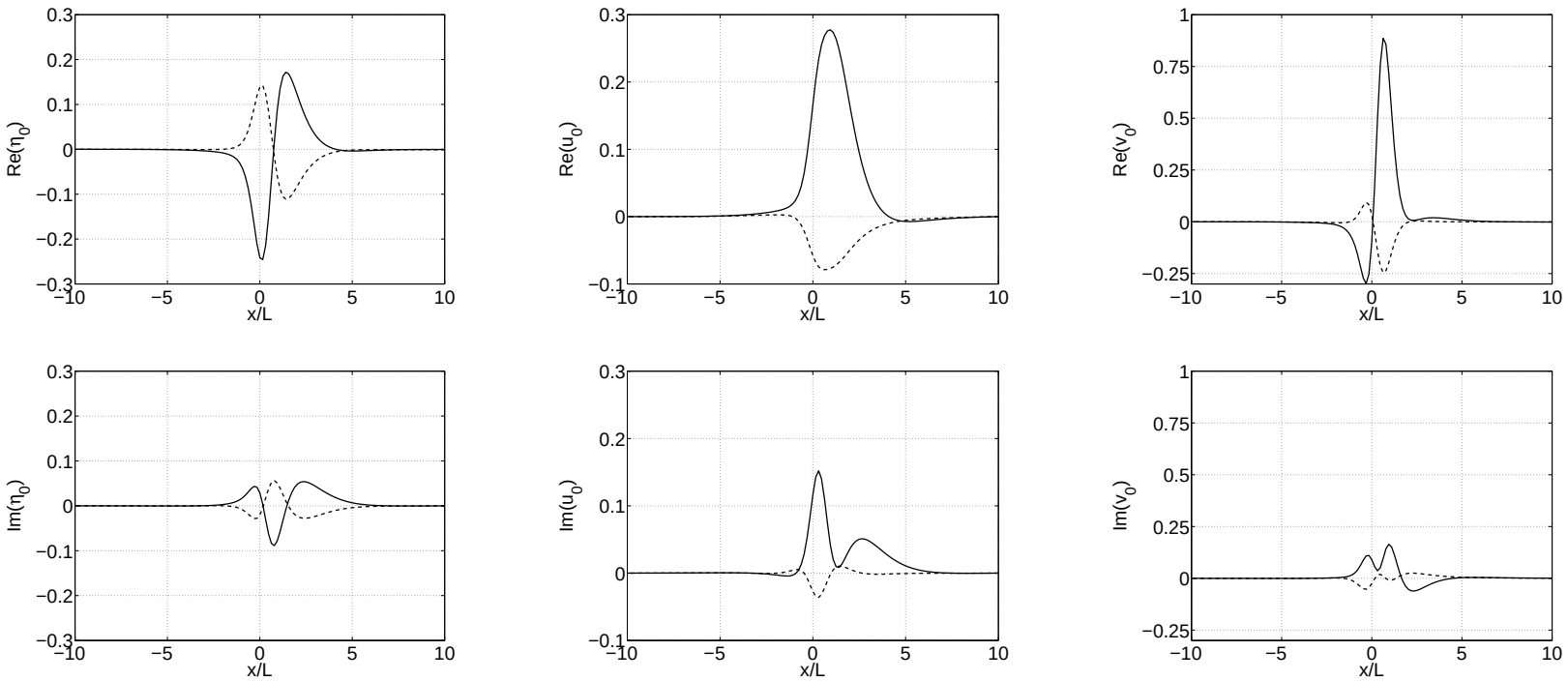

Striking resemblance to 1D II mode.

2D structure of the most unstable mode

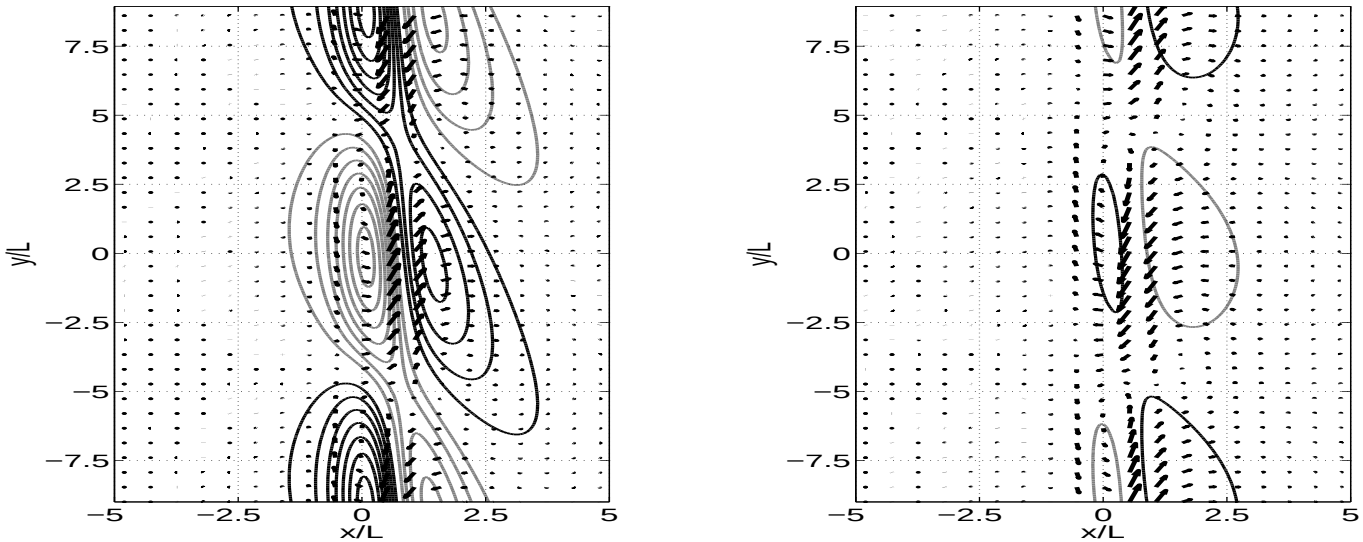

Essentially baroclinic, concentrated in the anticyclonic shear.

Cross-section at $y = 0$ of the second-unstable mode

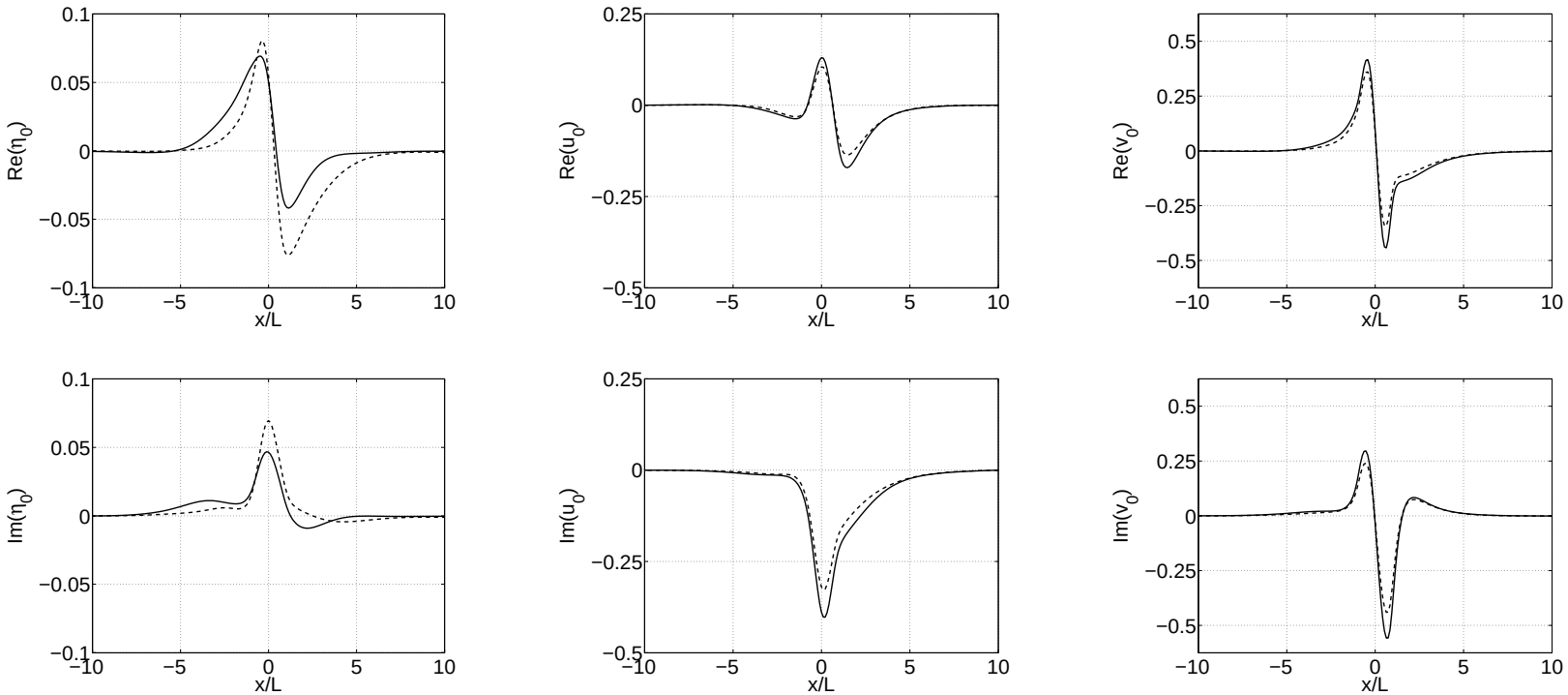

Essentially barotropic.

2D structure of the second-unstable mode

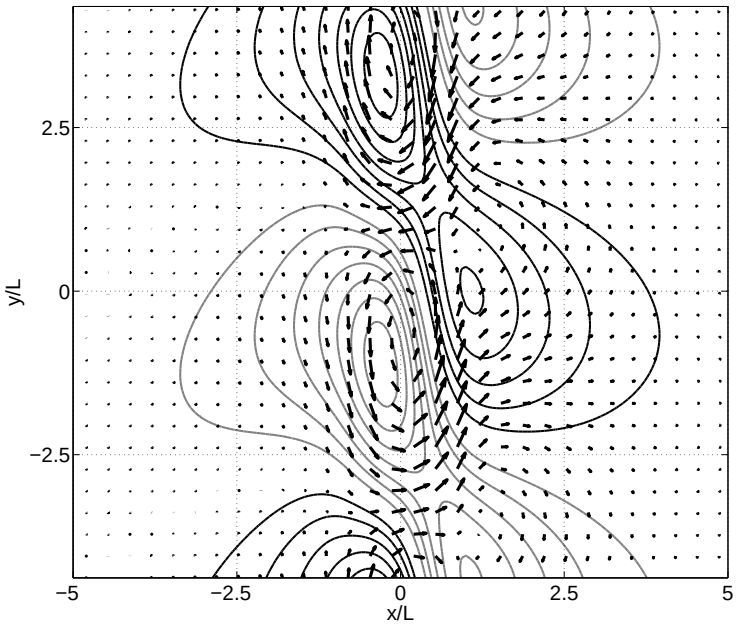

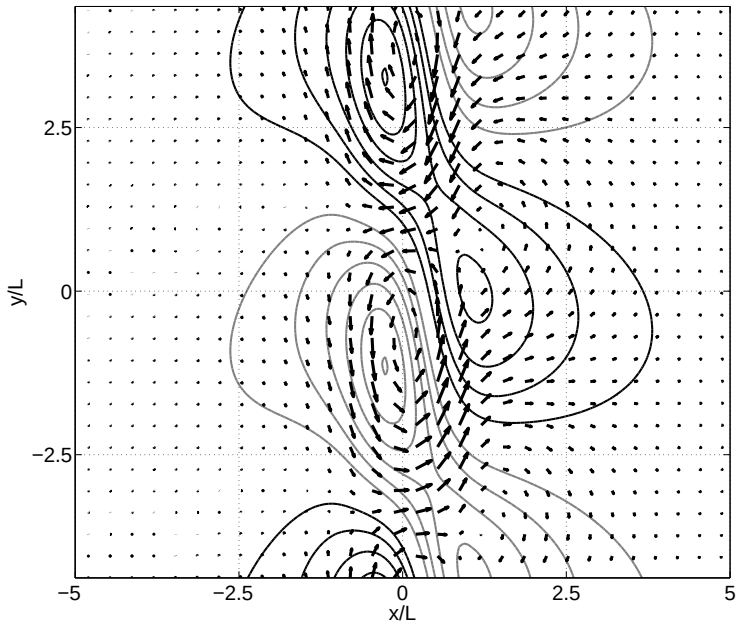

Early stages of nonlinear evolution of *AII*: thickness

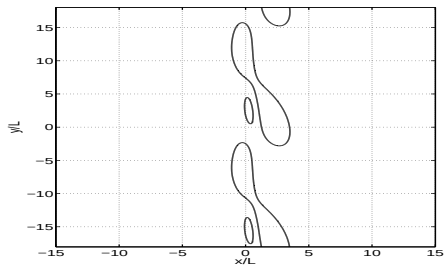

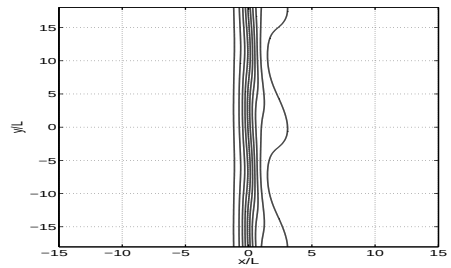

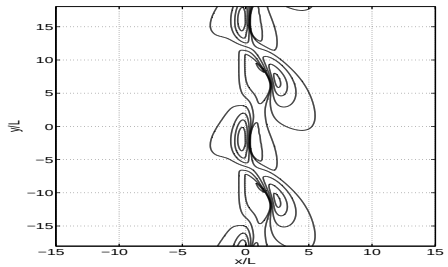

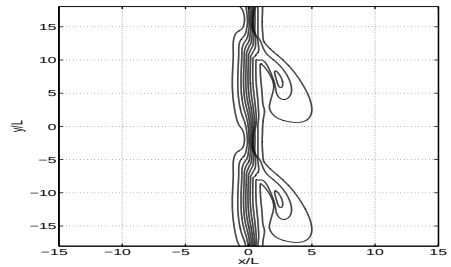

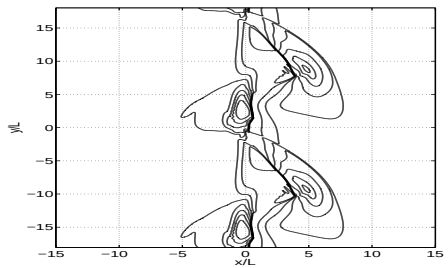

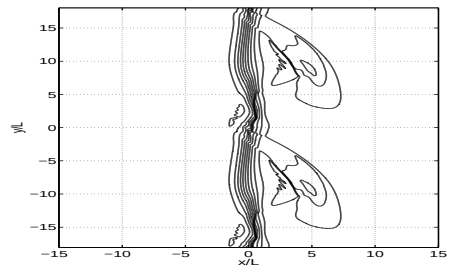

Early stages of nonlinear evolution of *AII*: vertical shear and PV

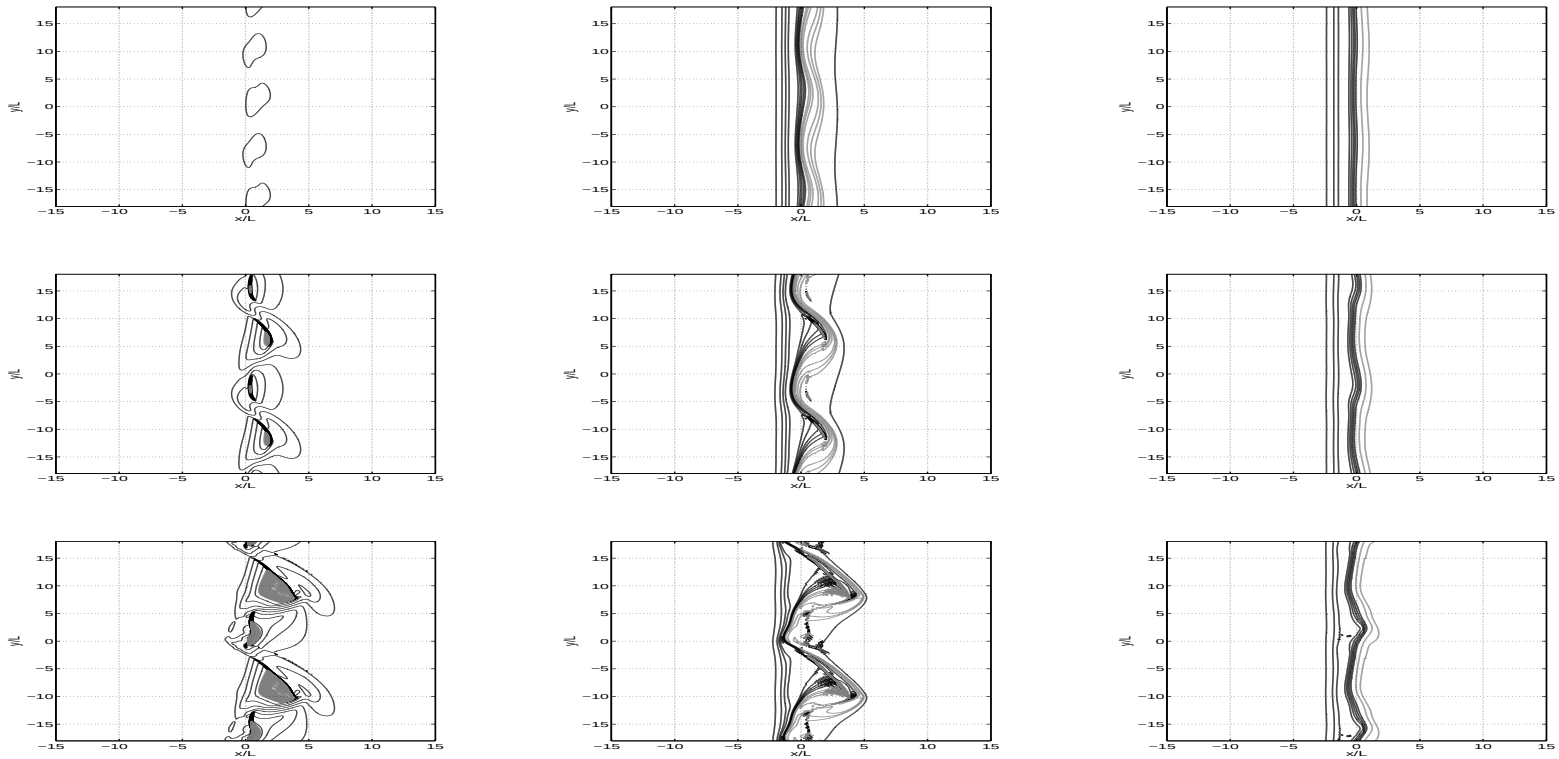

Late stages of nonlinear evolution of *AII*: thickness

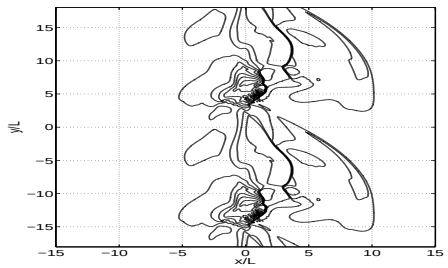

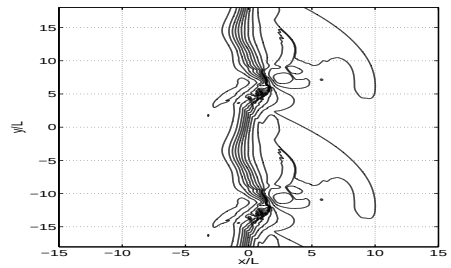

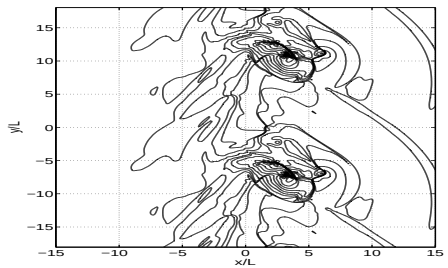

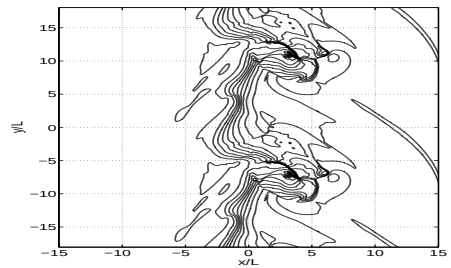

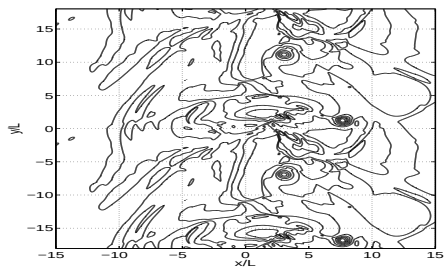

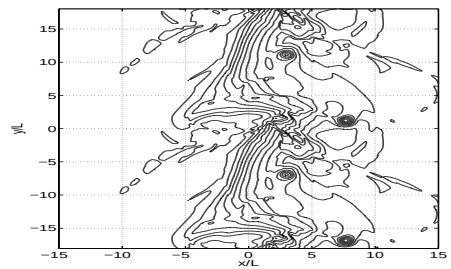

Late stages of nonlinear evolution of *AII*: vertical shear and PV

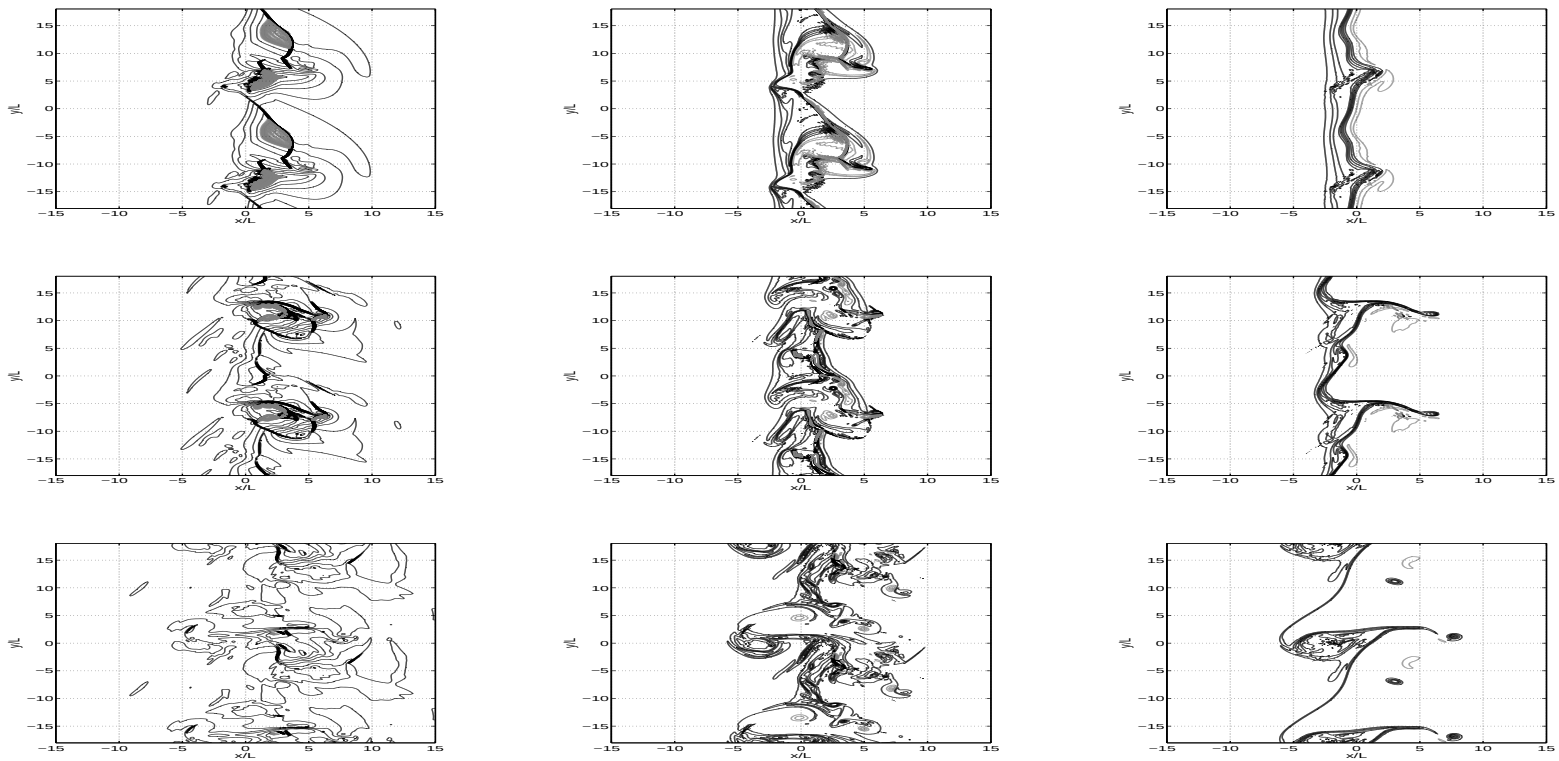

Loss of hyperbolicity

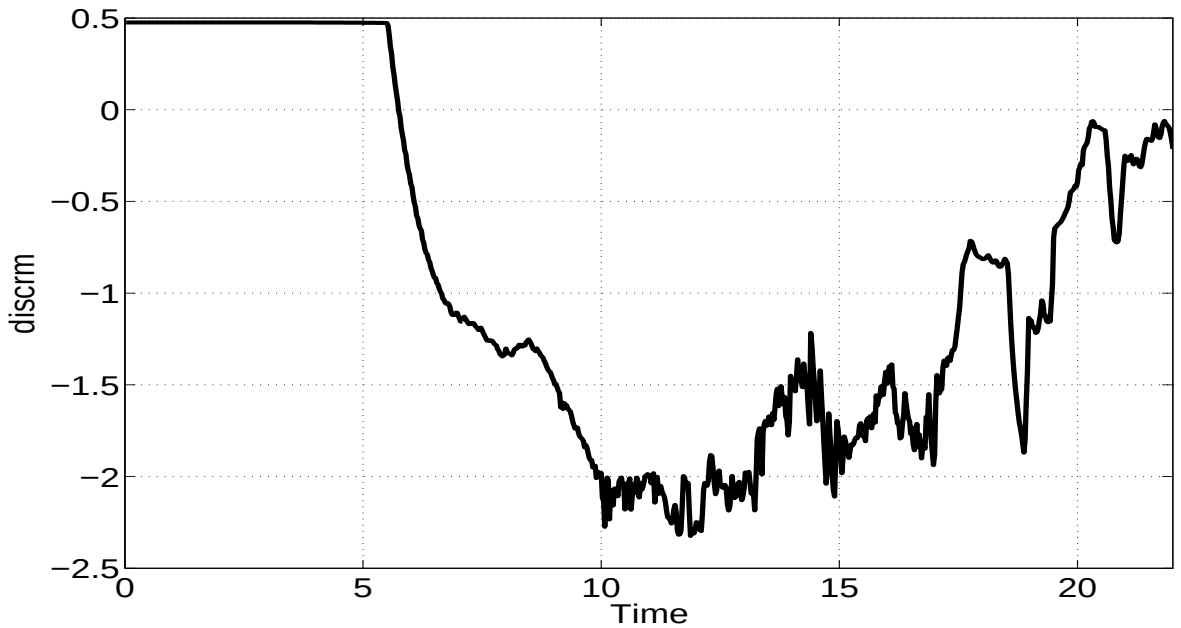

Time evolution of the minimum (over the whole calculation domain) of the discriminant of the characteristic matrix.

Energetics of the saturation

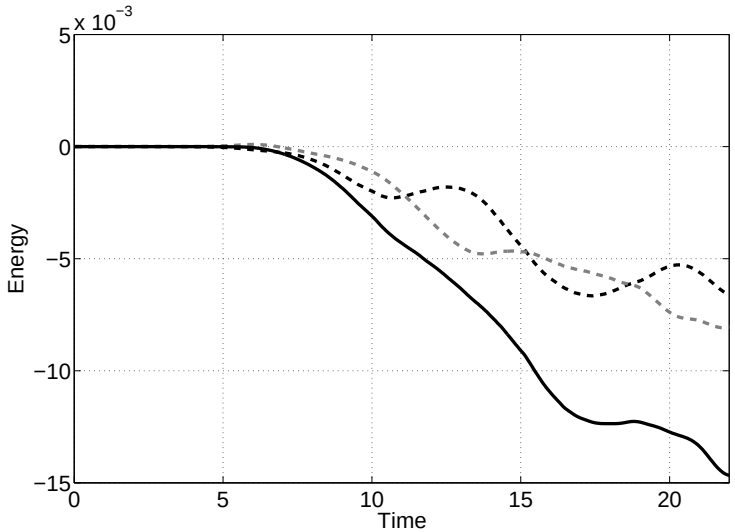

Normalized deviation of the total *(solid)*, kinetic *(black dashed)*, and potential *(gray dashed)* energy from their initial values.
"Inverse" (kinetic $\rightarrow$ potential) budget.

Intensification of ageostrophic motions

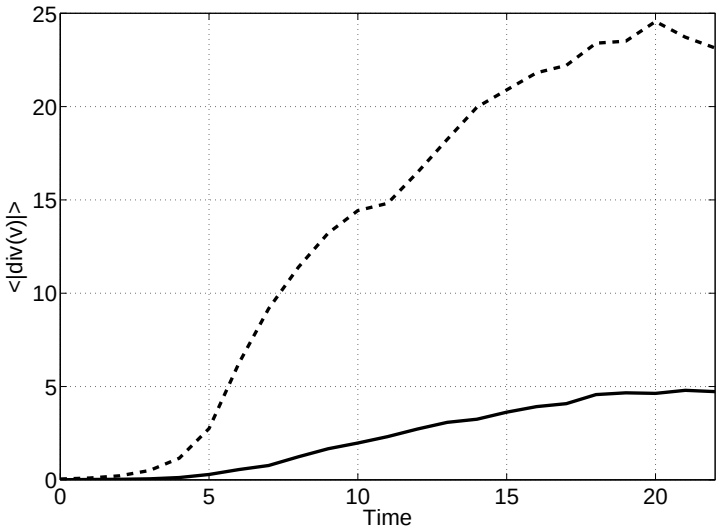

Evolution of the norm of ageostrophic motions. Baroclinic (*dotted)* and barotropic (*solid)* component.

AII as a source of inertia-gravity waves

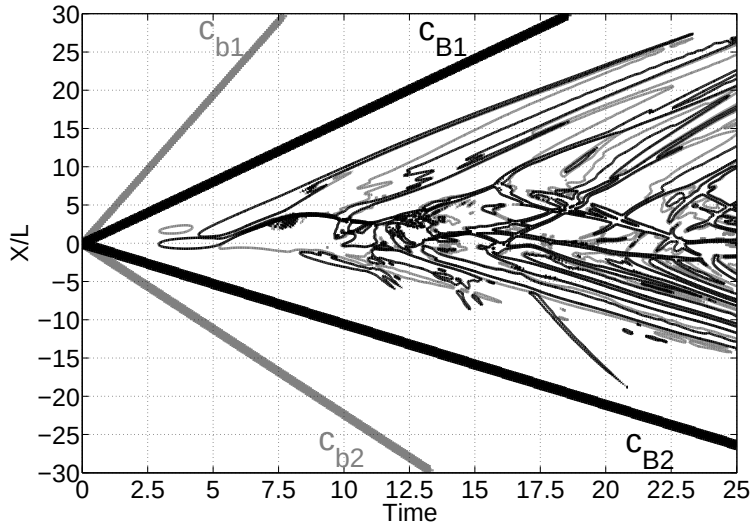

Hovmöller diagram of the baroclinic divergence field at $y = 0$.
Typical values $+0.1$ (black) and -0.1 (gray).
Spectrum of y - averaged divergence norm at $x/L = \pm 20$ integrated over supra-inertial motions: $\approx 60\%$ of the whole integrated spectrum.

Saturation of ageostrophic *BTI*: vertical shear and PV

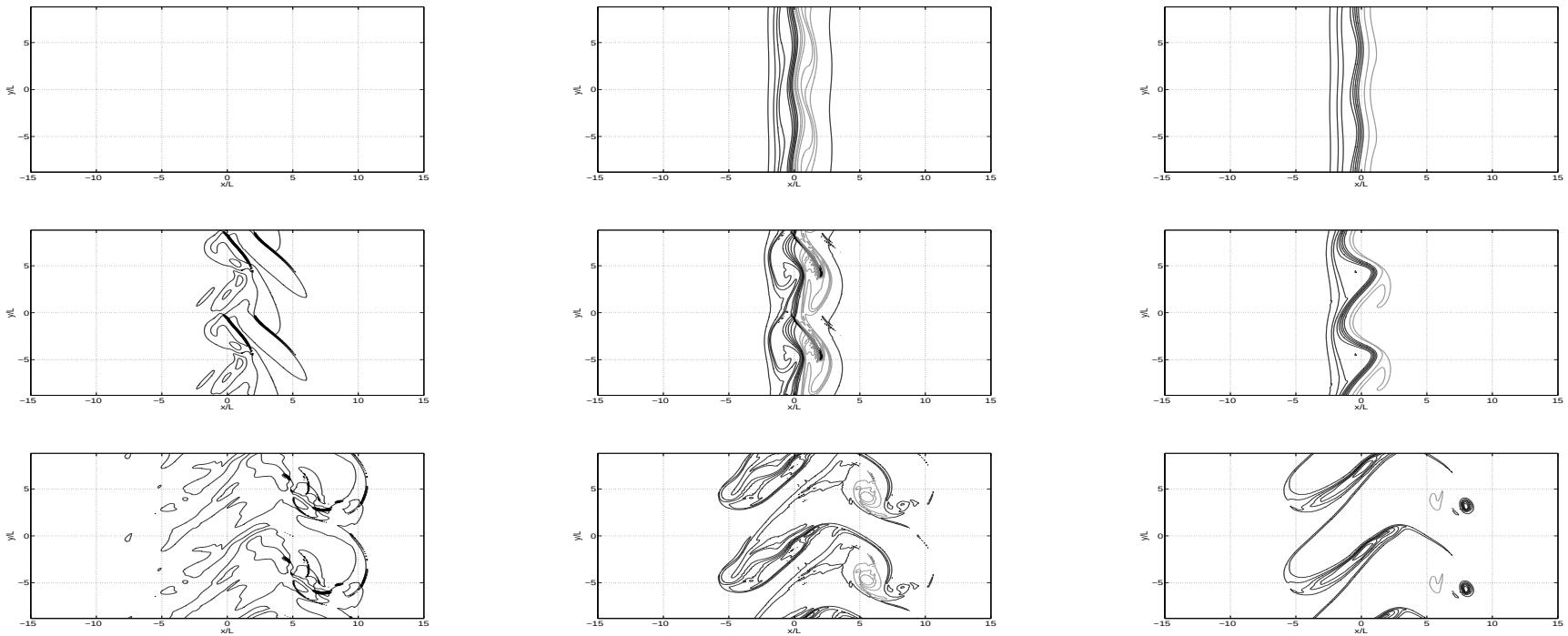

Hyperbolicity loss

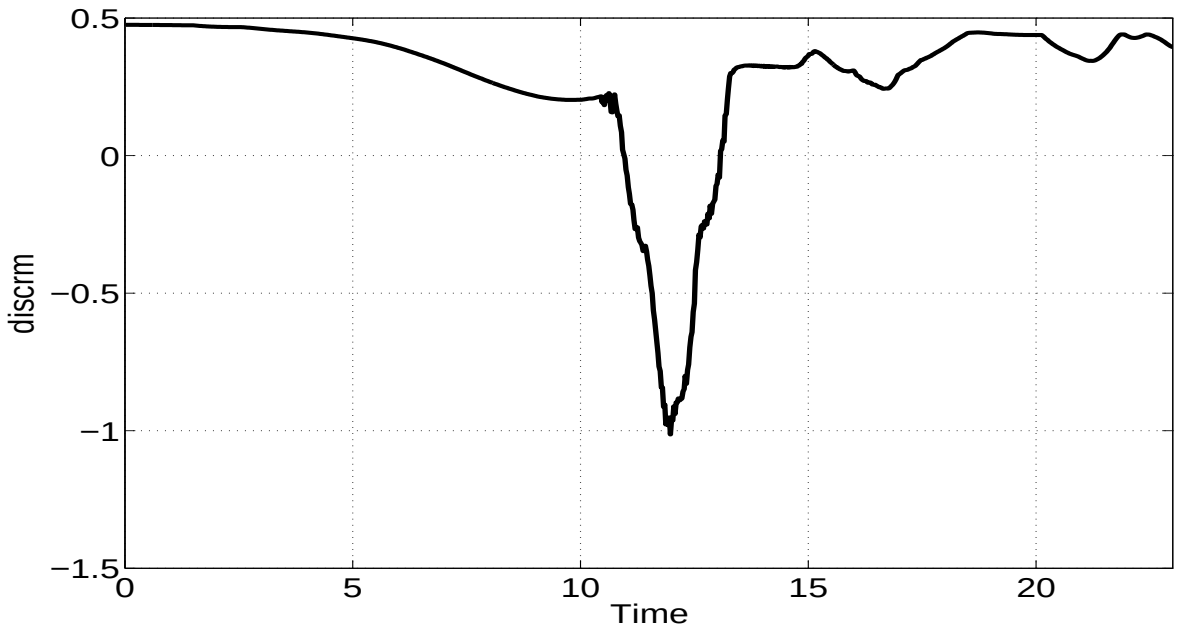

Time evolution of the minimum (on the whole calculation domain) of the discriminant of the characteristic matrix.

Energetics of the saturation

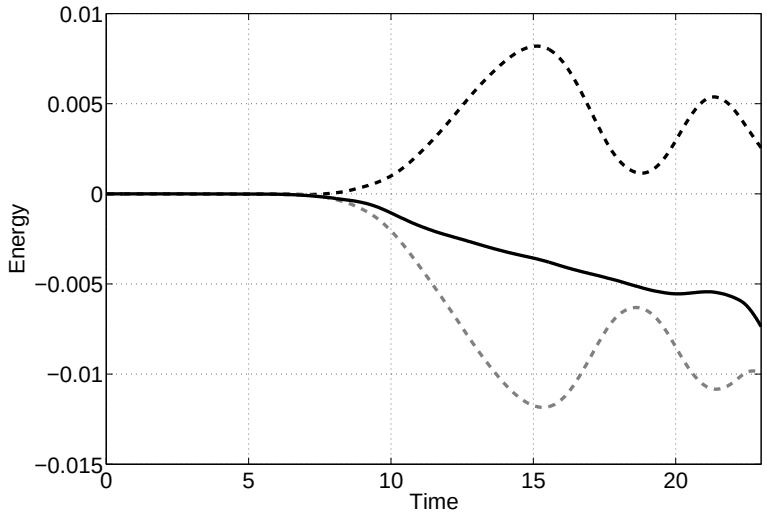

Normalized deviation of the total *(solid)*, kinetic *(black dashed)*, and potential *(gray dashed)* energy from their initial values.
"Direct" (potential $\rightarrow$ kinetic) budget.

Intensification of ageostrophic motions

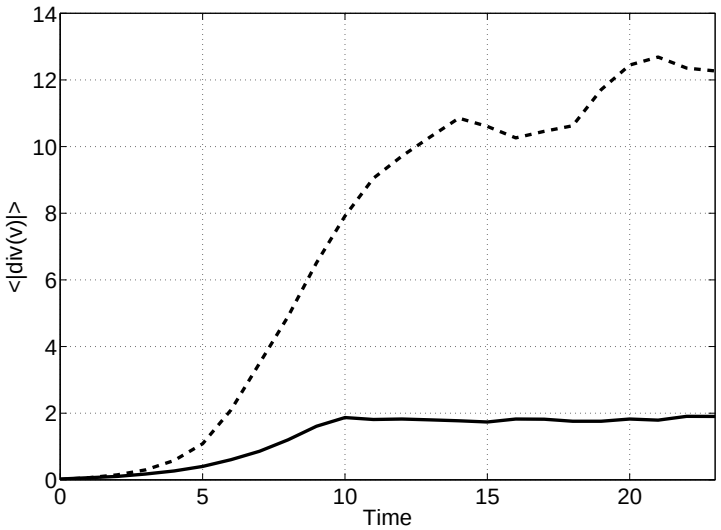

Evolution of the norm of ageostrophic motions. Baroclinic (*dotted)* and barotropic (*solid)* component.

Saturation of the geostrophic *BCI*

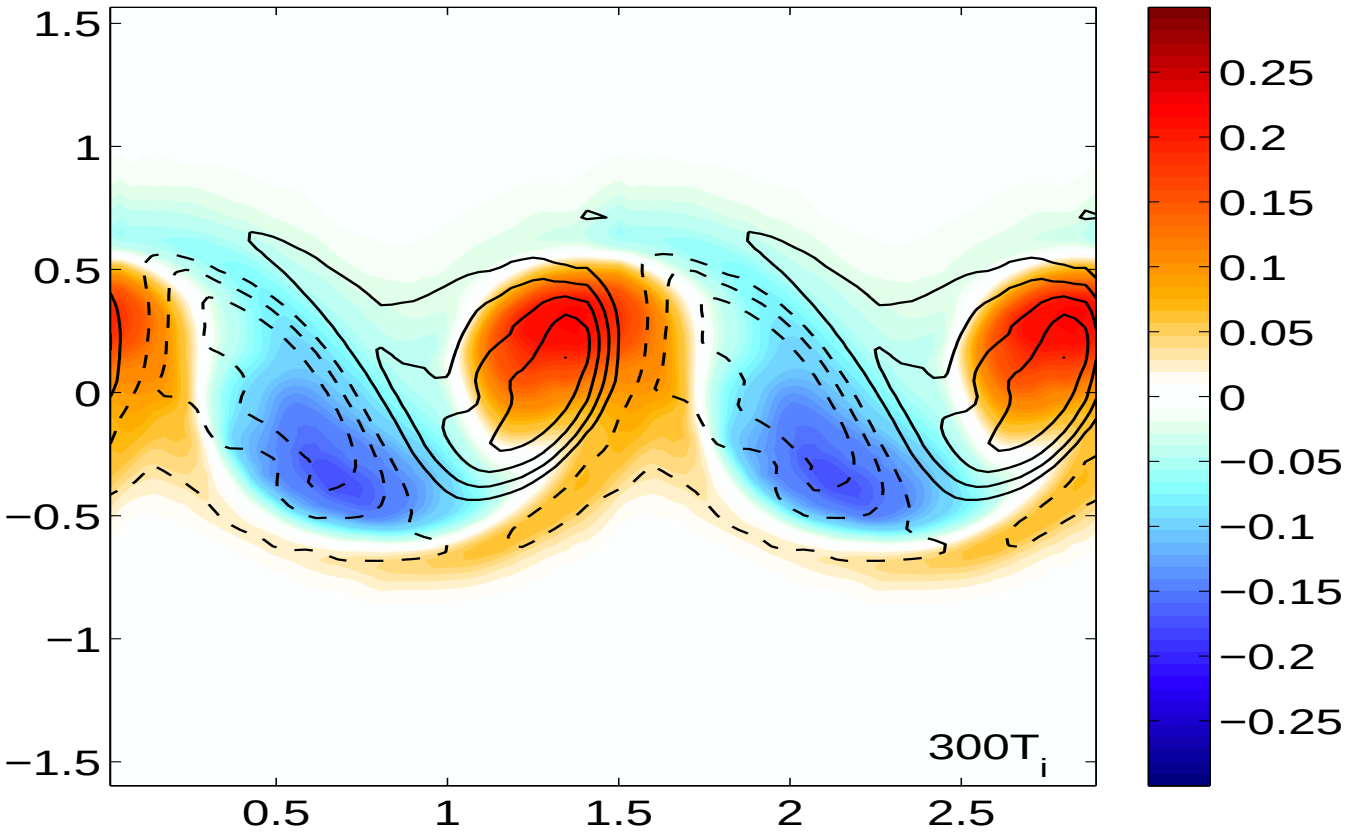

Relative vorticity. Colors: lower, contours: upper layer.

Summary of the 2-layer f-plane results I

- The leading long-wave instability of essentially ageostrophic jet is asymmetric inertial (*AII*). The most unstable mode is:
  1. baroclinic with dipolar cross-jet structure
  2. localized at the anticyclonic side of the jet
  3. tends to the eigenmode of symmetric inertial instability at $k \to 0$, but has a larger growth rate
- At the nonlinear stage AII produces small-scale structures and strong shears leading to enhanced dissipation. Considerable emission of IGW observed.

Summary of the 2-layer *f*-plane results II

- The second-leading instability is barotropic (*BTI*)
- With diminishing *Ro* a mode swap takes place with
  1. barotropic instability becoming most unstable
  2. monopolar baroclinic mode becoming second-unstable
  3. dipolar barotropic mode becoming third-unstable
- A region of wavenumbers exist where *AII* and *BTI* compete

Motivations

- Inertial instability most natural in equatorial region due to vanishing f
- Zonal jets ubiquitous at equator, their instabilities determine much of dynamics
- Systematic studies of the instabilities of equatorial jets scarce
- Instabilities can be viewed as linear resonances of waves supported by the sytem - vast variety of equatorial waves, as compared to the f - plane

Governing equations

2-layer RSW

$$\begin{aligned} D_{it}\vec{v_i} + \beta y \vec{e_z} \times \vec{v_i} + g\vec{\nabla}(\rho_i h_1 + h_2) &= 0\,, \\ \partial_t h_i + \partial_x(h_i u_i) + \partial_y(h_i v_i) &= 0\,. \end{aligned} \tag{3.1}$$

where the index $i = 1, 2$ refers to the upper and the lower layers, respectively, $D_{it} = \partial_t + u_i\partial_x + v_i\partial_y$ are advective derivatives in the layers, $\rho_1 \equiv 1$, $\rho_2 = \rho < 1$, are the densities of the layers, and $\vec{v_i}$, h_i are velocities and thicknesses of the layers.

Background flow

Barotropic Gaussian jet

$$\begin{aligned} H_1(y) &= H_{10}\ , \\ H_2(y) &= H_{20} - \Delta H e^{-(y/L)^2}\ , \\ U_1(y) &= -2U_0 e^{-(y/L)^2}\ , \\ U_2(y) &= -2U_0 e^{-(y/L)^2}\ , \\ V_1(y) &= V_2(y) = 0\ , \end{aligned} \tag{3.2}$$

where $\Delta H \leq H_{20}$ and $U_0 = \frac{g\Delta H}{\beta L^2}$. The dimensionless parameters are the Rossby number, the Burger number, and $d_i = \frac{H_{i0}}{H_0}$. We also introduce the parameters $\lambda = \frac{\Delta H}{H_0} = \frac{Ro}{Bu}$ (necessarily, $d_2 \geq \lambda$), and $d = \frac{H_{10}}{H_{20}}$.

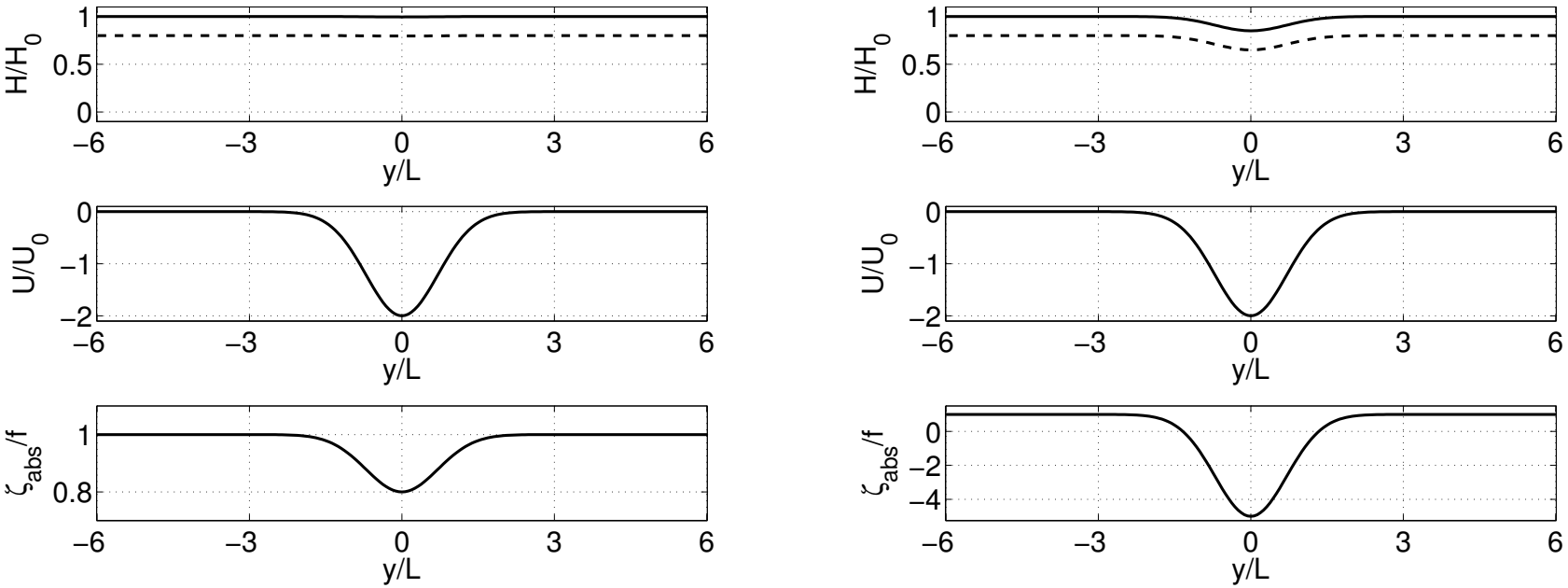

Background flow with $Bu = 10$, $\rho = 0.5$ and $d = 0.25$ at $Ro = 0.05$ (left column) and $Ro = 1.5$ (right column) with $\lambda = \frac{\Delta H}{H} = \frac{Ro}{Bu} = 5 \times 10^{-3}$ or 0.15, resp.. *Top:* thicknesses of the layers; *Middle:* zonal velocity profile (same in 2 layers); *Bottom:* profile of the absolute vorticity normalized by the planetary vorticity $\frac{\beta y + \zeta}{f}$ (same in 2 layers)

Stable configuration $Ro = 0.05$. Wave spectrum.

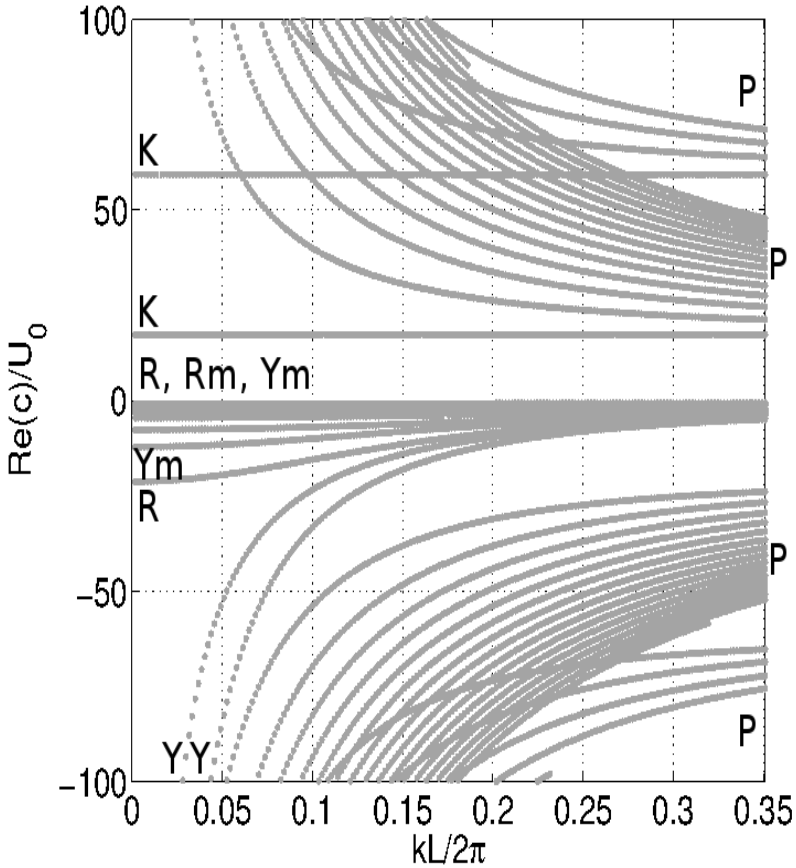

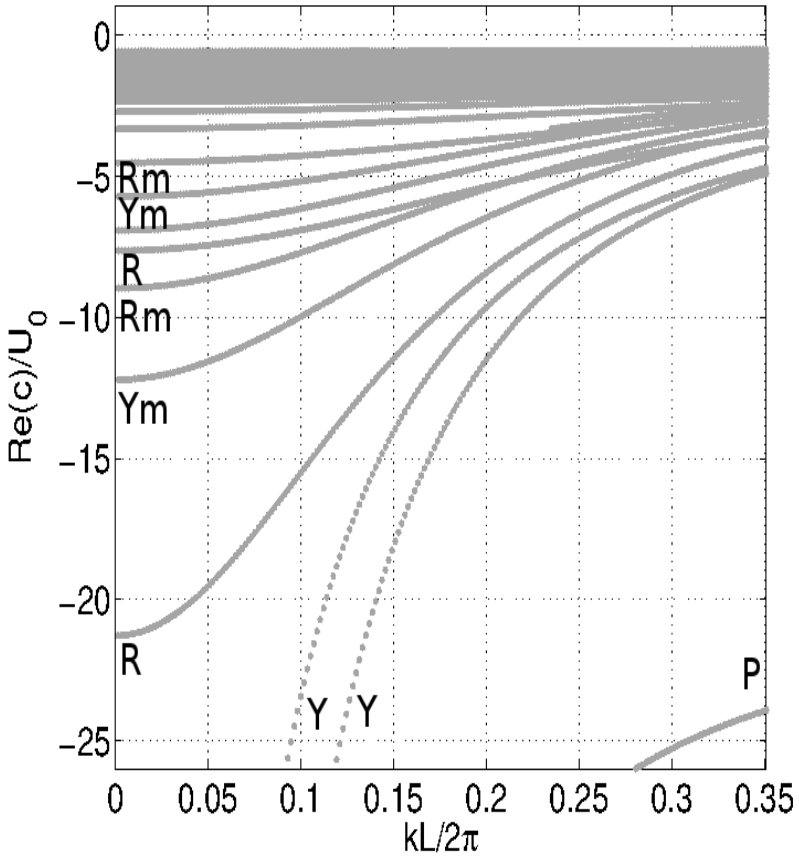

Example of a phase-portrait: baroclinic and barotropic Yanai waves

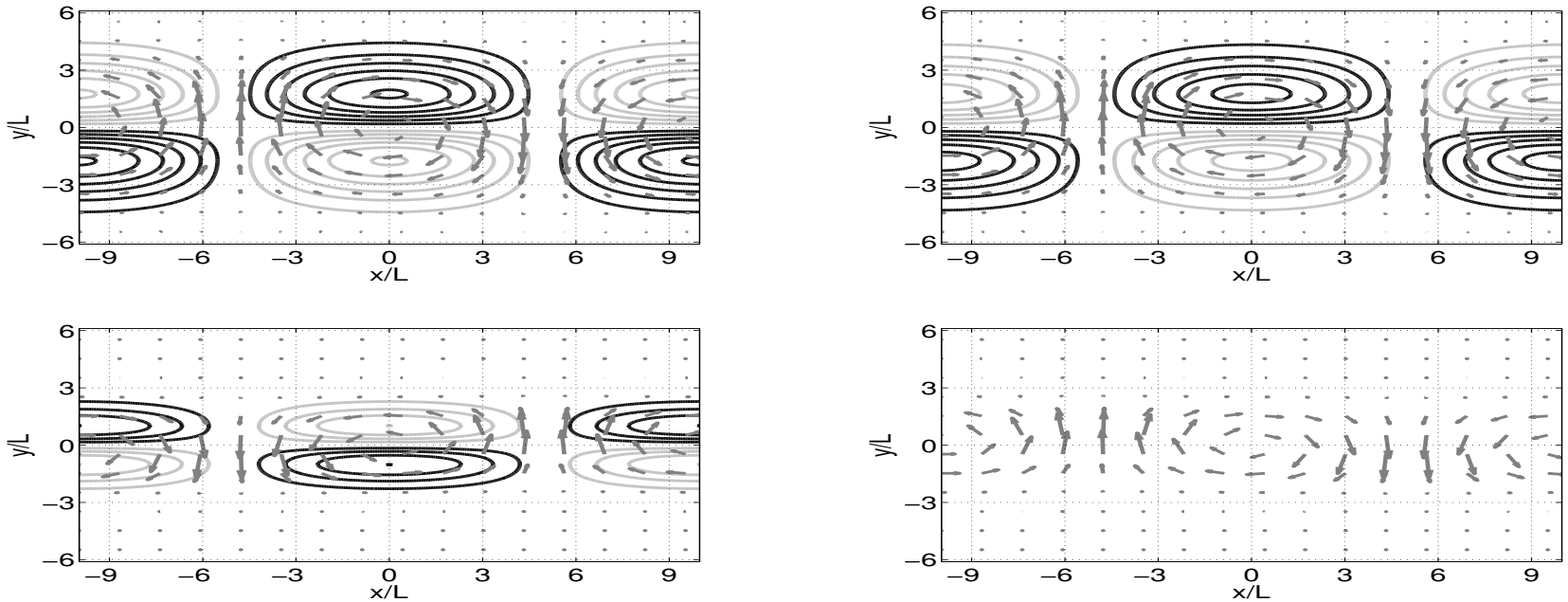

Upper: - barotropic, *Lower:* - baroclinic

Stability diagram for $Ro = 0.27$, $\rho = 0.5$, $d = 0.25$

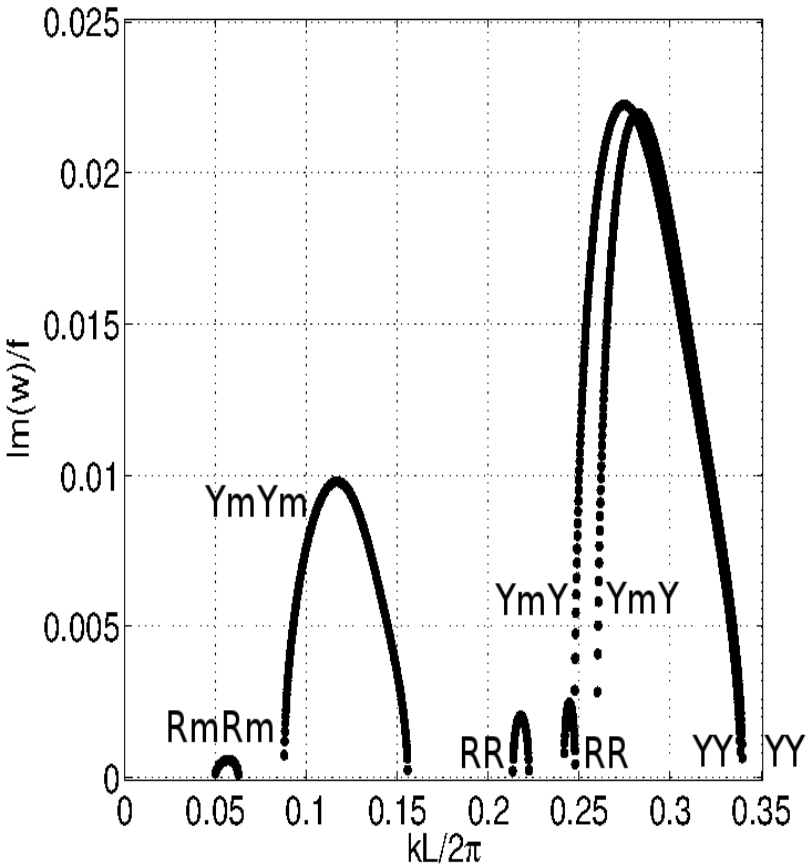

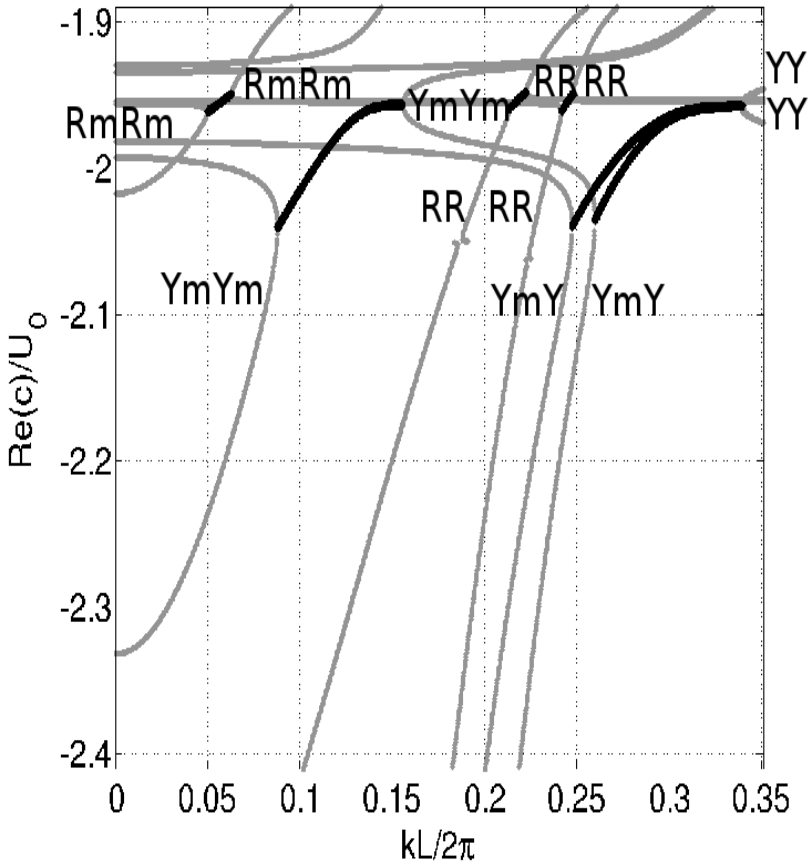

Evolution of stability diagrams from $Ro = 0.5$ to $Ro = 1.5$ and appearance of symmetric *II*

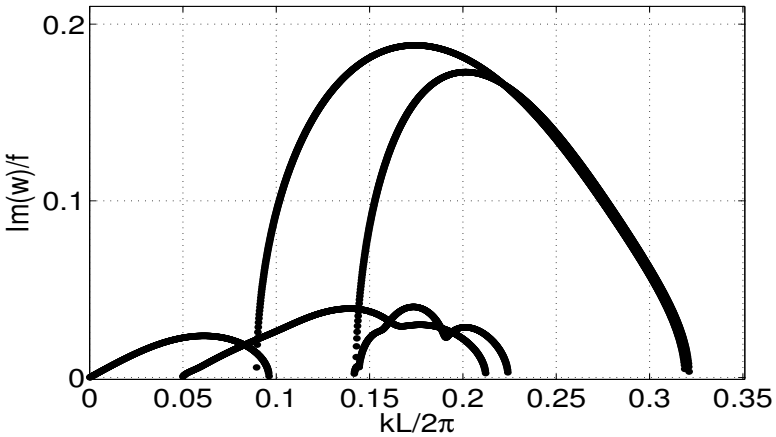

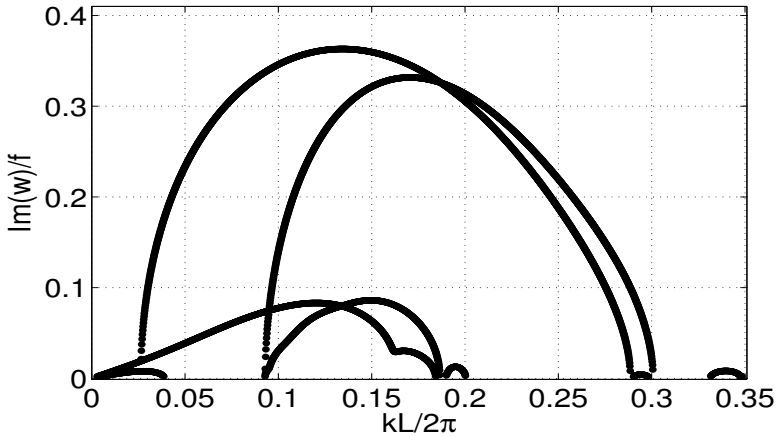

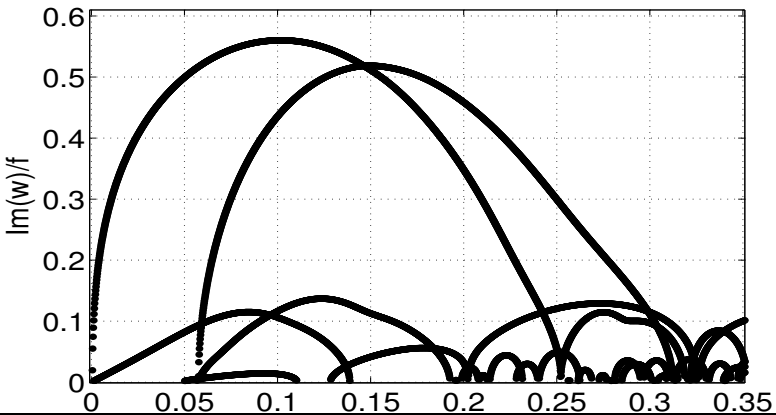

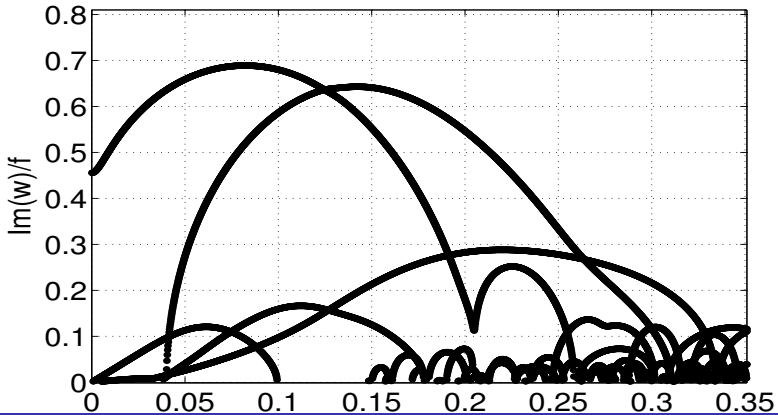

Phase-portrait of the most unstable mode at $Ro = 1.5$

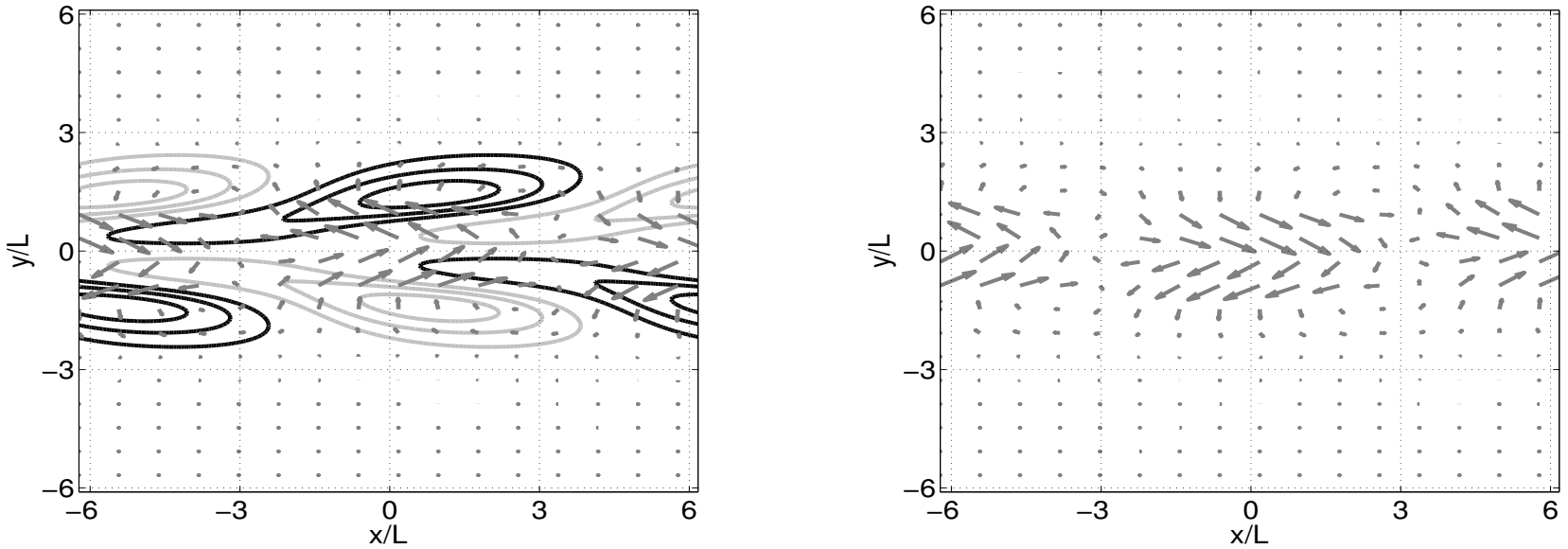

Left: - upper, *Right:* - lower layer

A résumé of the linear stability analysis in the two-layer model

Barotropic Gaussian easterly jet in equatorial 2-layer model is stable at small Rossby numbers but loses stability at $Ro \simeq 0.25$. Dominant instabilities are due to phase-locking and resonances between a pair of barotropic, or a pair of baroclinic Yanai-type waves propagating on the background of the jet. Standard barotropic and baroclinic instabilities due to resonances of Rossby waves are present, but are weaker. With increasing Ro the baroclinic YY - instability overcomes the barotropic one, and the wavenumber of the most unstable mode diminishes. At high enough Ro this instability has nonzero growth rate at $k = 0$, giving a standard symmetric inertial instability. Yet the maximal growth rate is achieved at small but non-zero k.

Saturation of the most unstable mode at $Ro = 1.5$. Relative vorticity - upper layer.

$t = 5/\beta L$

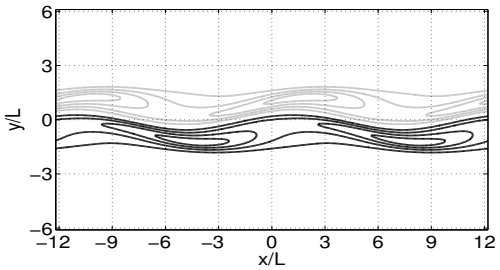

$t = 7/\beta L$

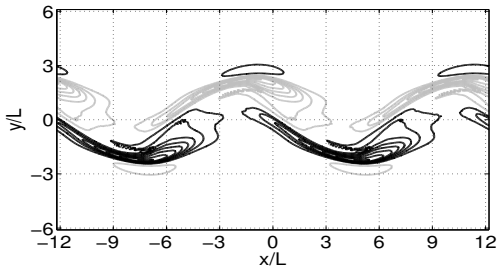

$t = 10/\beta L$

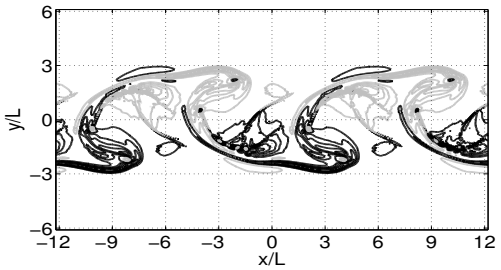

$t = 14/\beta L$

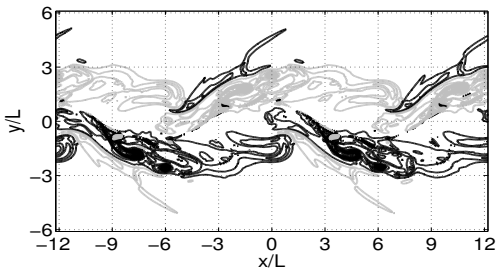

$t = 19/\beta L$

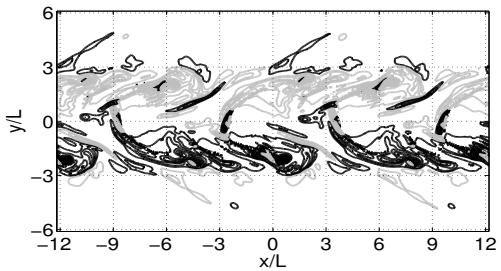

$t = 28.5/\beta L$

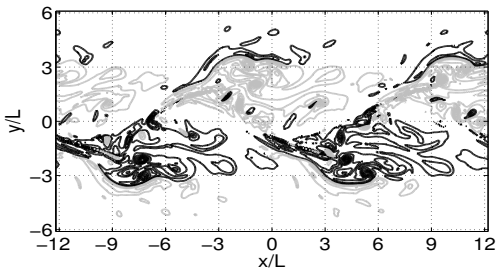

Saturation of the most unstable mode at $Ro = 1.5$. Relative vorticity - lower layer.

$t = 5/\beta L$

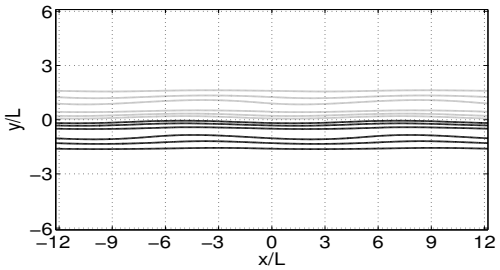

$t = 7/\beta L$

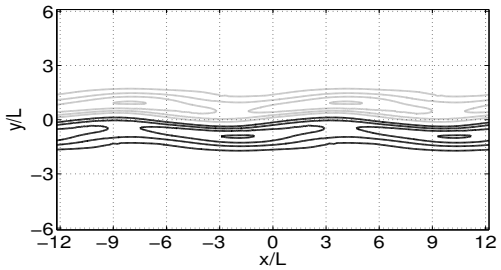

$t = 10/\beta L$

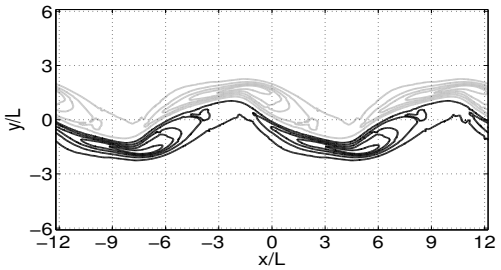

$t = 14/\beta L$

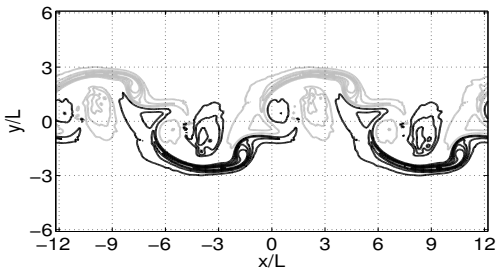

$t = 19/\beta L$

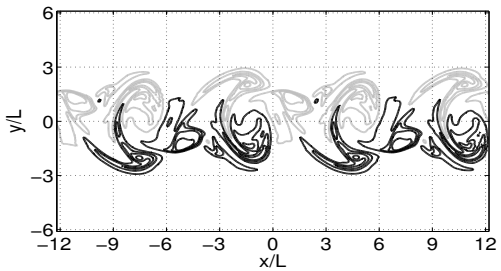

$t = 28.5/\beta L$

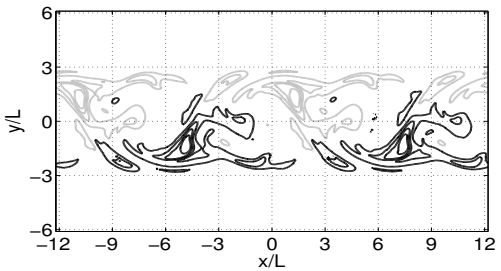

Saturation of the most unstable mode at $Ro = 1.5$. Energy evolution

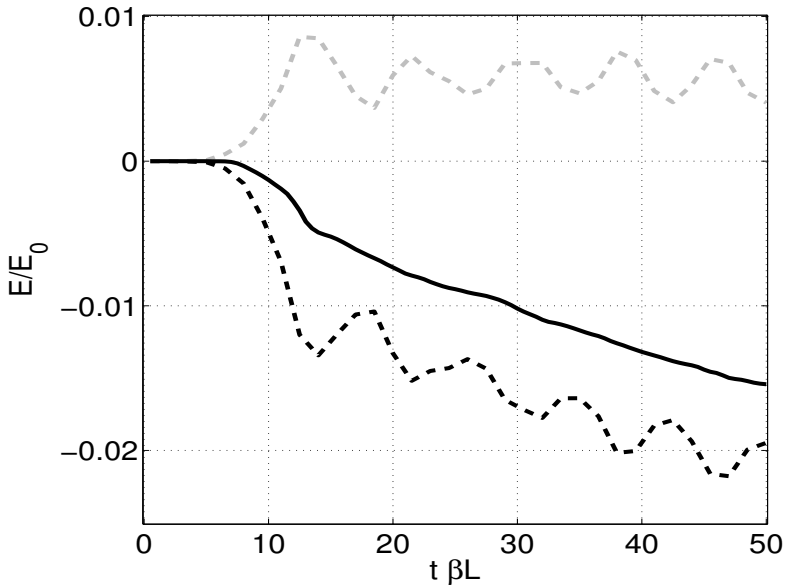

Solid: - total, *Dashed black:* - kinetic, *Dashed gray:* - potential energy.

Saturation of the most unstable mode at $Ro = 1.5$. Vertical shear and dissipation

$t = 5/\beta L$

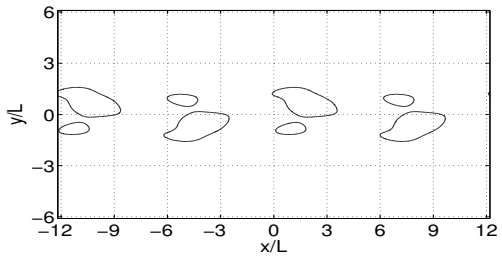

$t = 7/\beta L$

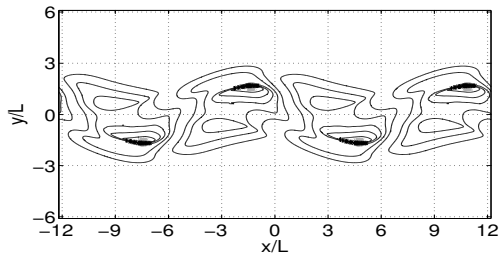

$t = 10/\beta L$

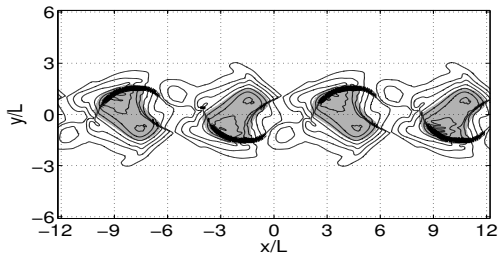

$t = 14/\beta L$

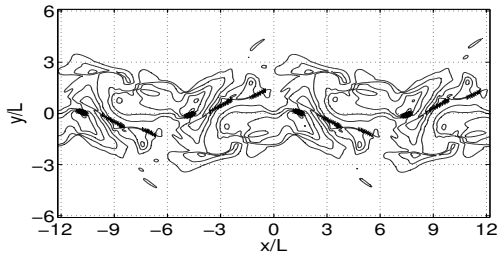

$t = 19/\beta L$

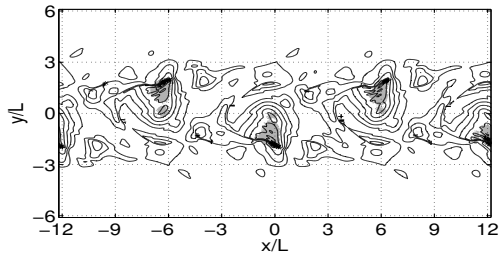

$t = 28.5/\beta L$

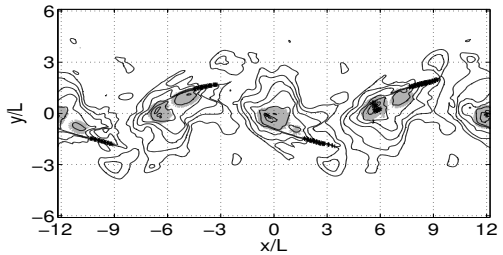

Velocity shear $|u_2 - u_1|$ *(thin black)*, enhanced dissipation zones *(black)* and zones of hyperbolicity loss *(gray)*.

Summary of the results at the equator

- The threshold of instability of easterly jets centered at the equator is at $Ro \approx 1/4$,
- Dominant barotropic and baroclinic instabilities are due to (modified) Yanai waves, and not Rossby waves as on the mid-latitude tangent plane
- Classical symmetric inertial insability is a particular case of essentially ageostrophic baroclinic instability arising at high enough Ro
- Asymmetric inertial instability is stronger than symmetric one
- Nonlinear saturation of the dominant instability at large Ro produces much mixing and strong dissipation, for small Ro nonlinear oscillations of the jet observed.

Goals and strategy

Goals:

- To understand how the results of 2-layer model are modified for continuous stratification
- To understand how *I I* and *B I* interact in fully 3D simulations

Strategy

- Detailed linear stability analysis of the barotropic Bickley jet by the collocation method in a wide range of parameters
- Direct numerical simulations of the saturation of the inertially unstable jet with WRF model

The model

Continuously stratified primitive equations

$$\begin{aligned} D_t \vec{v}_h + \vec{f} \times \vec{v}_h + \vec{\nabla}_h \Phi_{tot} - \nu \partial_z^2 \vec{v}_h &= 0 , \\ D_t \theta_{tot} - \kappa \partial_z^2 \theta_{tot} &= 0 , \\ \partial_z \Phi_{tot} - g \frac{\theta_{tot}}{\theta_r} &= 0 , \\ \vec{\nabla}_h \vec{v}_h + \partial_z w &= 0 . \end{aligned} \tag{4.1}$$

Here $(\vec{v}_h, w)$ - 3 components of velocity, $\vec{v}_h = (u, v)$, $D_t = \partial_t + \vec{v}.\vec{\nabla}$, $\vec{f} = f\vec{k}$, ν and κ - vertical (turbulent) viscosity and diffusivity (set to zero in linear stability analysis).
Below: linear stratification $\theta_0(z) \to \Phi_0(z)$. $N^2 = \frac{g\partial_z \theta_0}{\theta_r} = \text{const}$, θ_r - a reference value.

Background flow

Barotropic Bickley jet:

Balanced solution of (4.1) $\Phi = \bar{\Phi}(y), u = \bar{u}(y), v = w = 0$:

$$\begin{aligned} \bar{\Phi}(y) &= -gH \tan(y/L) \,, \\ \bar{u}(y) &= \frac{gH}{fL}(1 - \tan^2(y/L)) \,. \end{aligned} \tag{4.2}$$

Scales and parameters

L and gH - width and intensity of the jet, $U_0 = \frac{gH}{fL}$ - peak velocity.

Dimensionless parameters:

- Burger number $Bu = \left(\frac{N}{f}\right)^2$,
- Rossby number $Ro = \frac{U_0}{fL} = \frac{gH}{(fL)^2}$,
- Aspect ratio $\delta = \frac{H}{L}$,
- "Ekman" number $\gamma = \frac{\nu}{fH^2}$.

Necessary condition for inertial instability: $f\bar{q} < 0$ (at the anticyclonic side of the jet) if $Ro > \frac{3\sqrt{3}}{4}$, where $\bar{q} = f - \partial_y \bar{u}$ is the vertical component of the absolute vorticity of the jet.

Barotropic Bickley jet

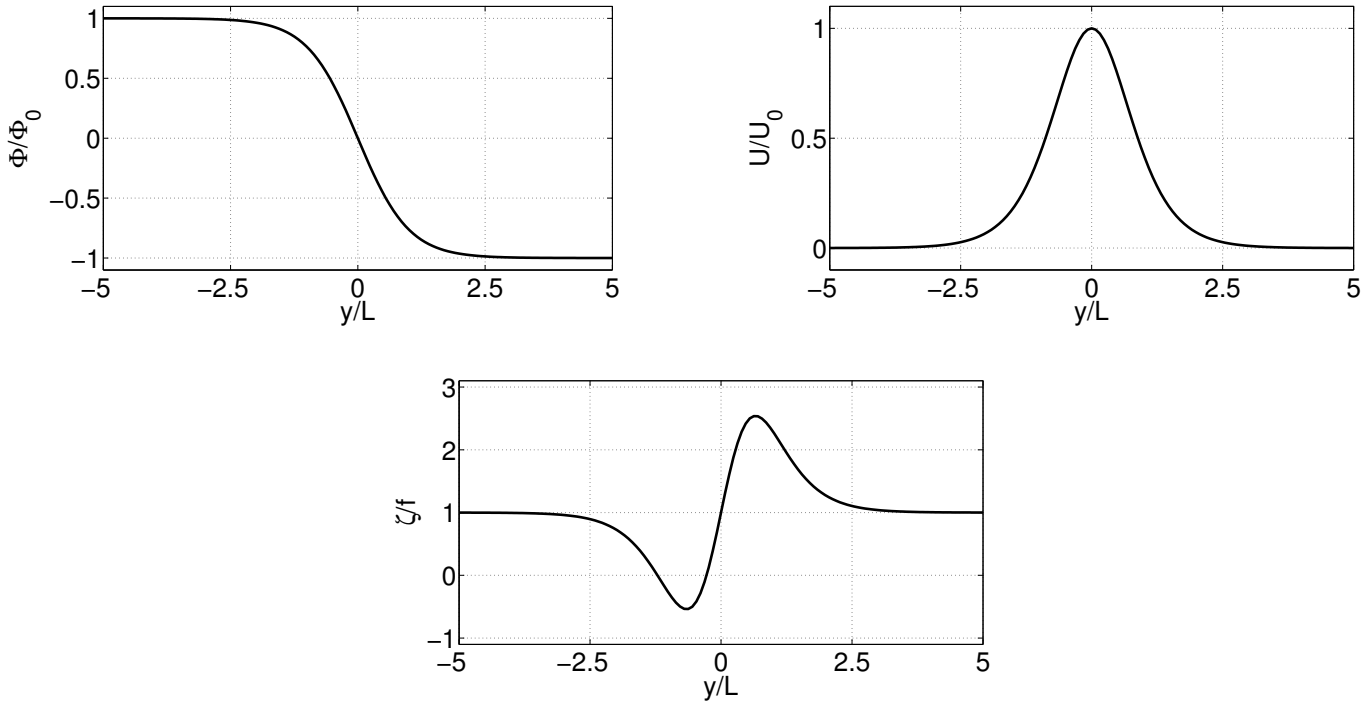

Cross-section of a jet with $Ro = 2$, $Bu = 1.9 \times 10^4$, $\delta = 1.08 \times 10^{-4}$. *Top left:* geopotential , *Top right:* velocity , *Bottom:* Vertical component of the normalized absolute vorticity

.

Linear stability analysis

Workflow

- Linearize equations (4.1) about the background jet
- Look for a solution in the form $\propto e^{i(\omega t - kx - mz)}$
- For each vertical mode m , and each downstream wavenumber k treat the eigenvalue problem for the phase speed $c = \omega/k$ by collocation method in y
- Plot stability diagrams for the phase speed $Re(c)$ and growth rate $Im(\omega)$ as functions of k for each m

Stability diagram for small *Ro*

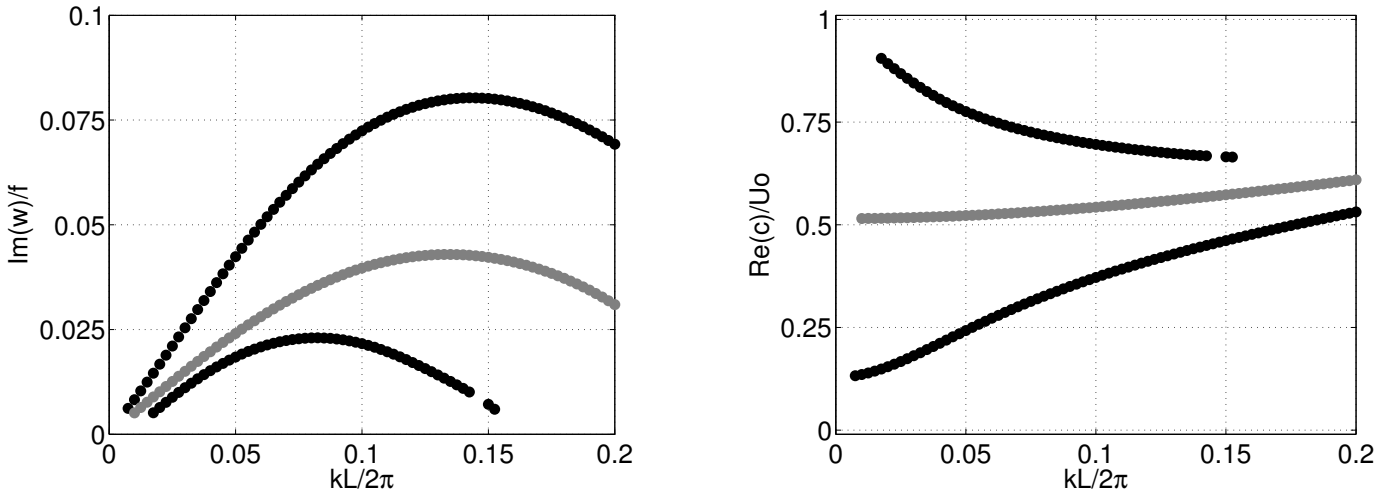

Linearly unstable modes of the jet at $Ro = 0.5$, $Bu = 1.9 \times 10^4$, $\delta = 0.27 \times 10^{-4}$ and $\gamma = 0$. *Left:* Normalized growth rate and *Right:* Normalized phase speed as functions of the downstream wavenumber k. *Black:* Vertical wavenumber $m = 1(\frac{2\pi}{L})$. *Gray:* Vertical wavenumber $m = 25(\frac{2\pi}{L})$.

2D structure of the most unstable modes

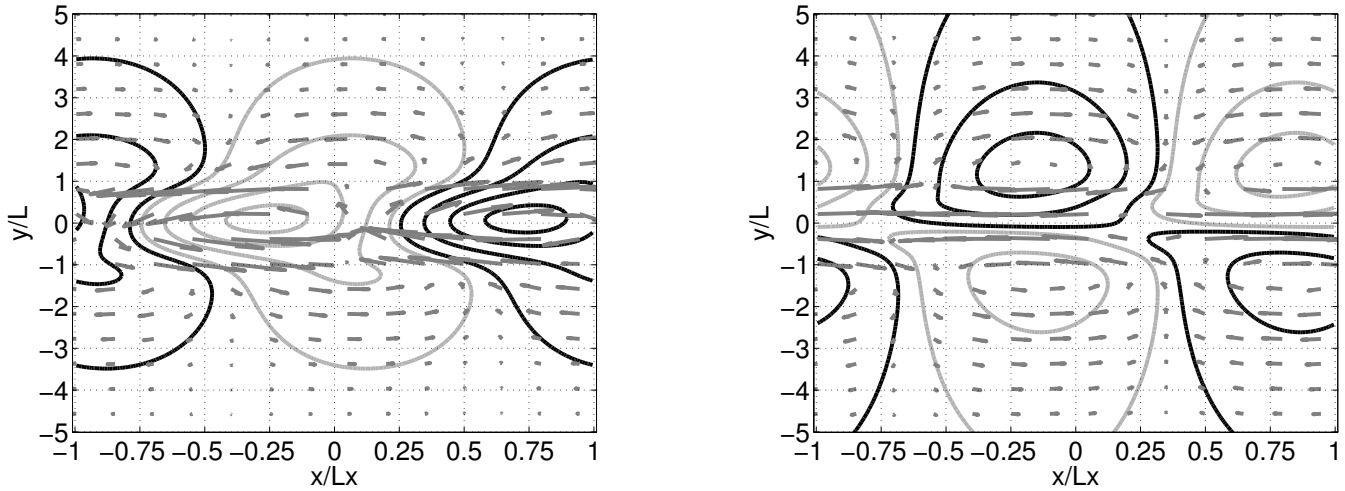

2D structure of the two most unstable modes of the jet with $Ro = 0.5$, $Bu = 1.9 \times 10^4$, $\delta = 0.27 \times 10^{-4}$ and $\gamma = 0$. Vertical wavenumber $m = 1(\frac{2\pi}{L})$. Isolines of geopotential and velocity (arrows) anomalies. Positive (negative) anomalies: gray (black). $L_x = \frac{\pi}{k}$. *Left:* most unstable mode ($k = 0.144(\frac{2\pi}{L})$). *Right:* less unstable mode ($k = 0.083(\frac{2\pi}{L})$).

Stability diagram for large *Ro*

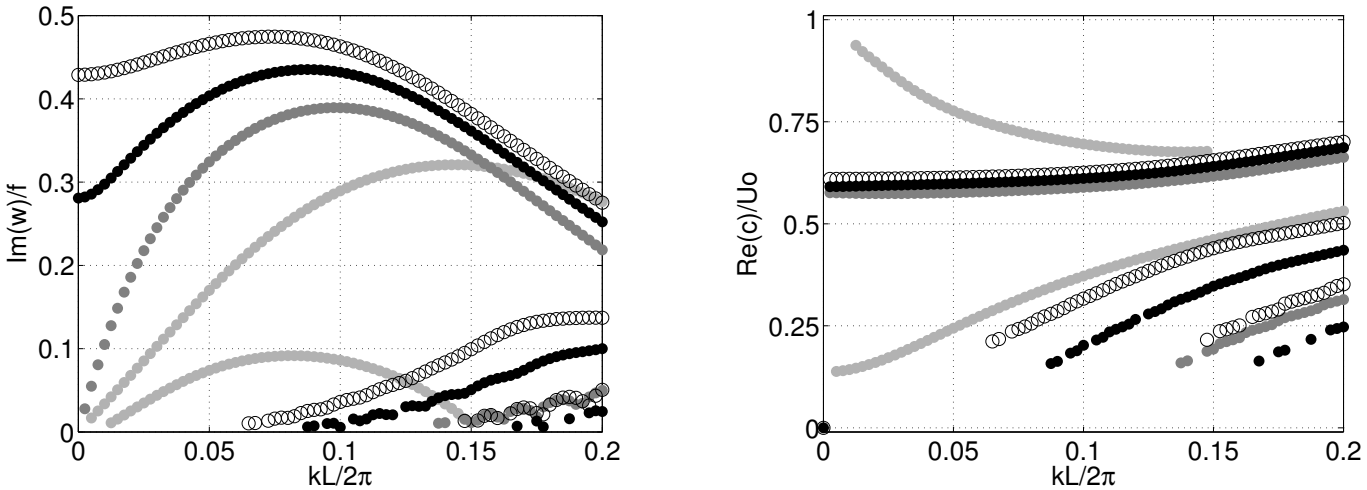

Linearly unstable modes of the jet at $Ro = 2$, $Bu = 1.9 \times 10^4$, $\delta = 1.08 \times 10^{-4}$ and $\gamma = 0$. *Left:* Normalized growth rate and *Right:* Normalized phase speed as functions of the downstream wavenumber k. *Light gray dots:* Vertical wavenumber $m = 1(\frac{2\pi}{L})$. *Gray dots:* $m = 50(\frac{2\pi}{L})$. *Black dots:* $m = 75(\frac{2\pi}{L})$. *Circles:* $m = 100(\frac{2\pi}{L})$.

2D structure of the most unstable modes

$m = 1(\frac{2\pi}{L})$

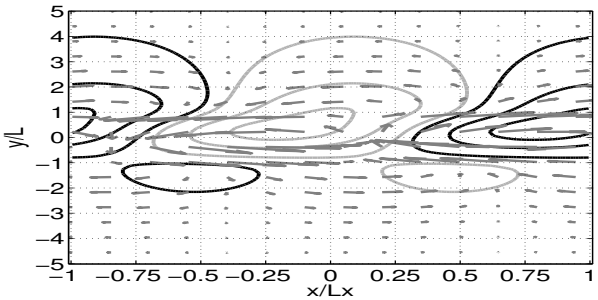

$m = 50(\frac{2\pi}{L})$

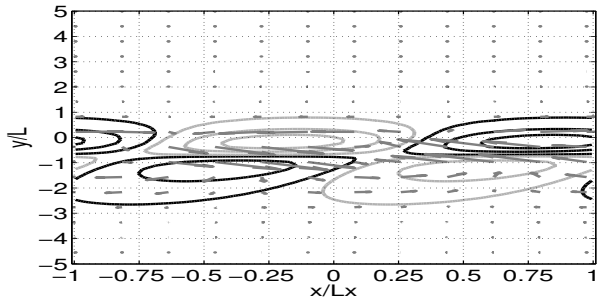

$m = 75(\frac{2\pi}{L})$

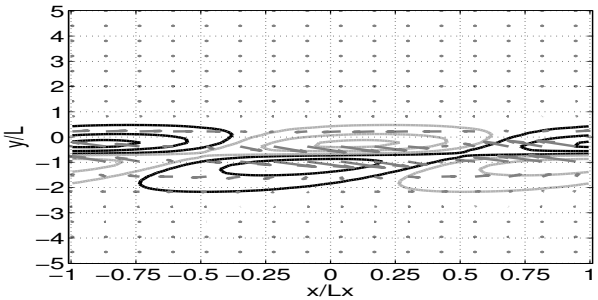

$m = 100(\frac{2\pi}{L})$

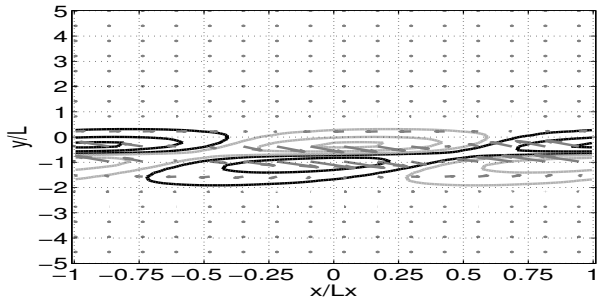

Most unstable modes of the jet with $Ro = 2$, $Bu = 1.9 \times 10^4$, $\delta = 1.08 \times 10^{-4}$ and $\gamma = 0$.

Constructing initial state

To avoid influence of vertical boundaries: barotropic unstable jet in the center of the domain, becoming stable at top/bottom:

$$U(y,z) = U_0(1-\tan^2(y/L))e^{-(\frac{z-H_{tot}/2}{H_{tot}/3})^2},$$

$\frac{U_0}{fL} = 2$ ($U_0 = 15m/s$). Thermal wind balance $\rightarrow$ horizontal gradients of temperature in the regions of vertical shear. $L = 100km$, $f \approx 0.73 \times 10^{-4}s^{-1}$. Computational domain: $l_y = 30L$ (walls - negligible influence), $l_x = 10L$. Top: $H_{tot} = 9km \gg fL/N$, $N = 0.0101s^{-1}$, $Bu = 1.9 \times 10^{-4}$. Wind/temperature from thermal wind balance. Perturbation: white noise in cross-stream velocity. Resolution: $dx,\ dy = 0.03L$, $dz = 0.0056H_{tot}$, $f \times dt = 0.0015$.

Background jet

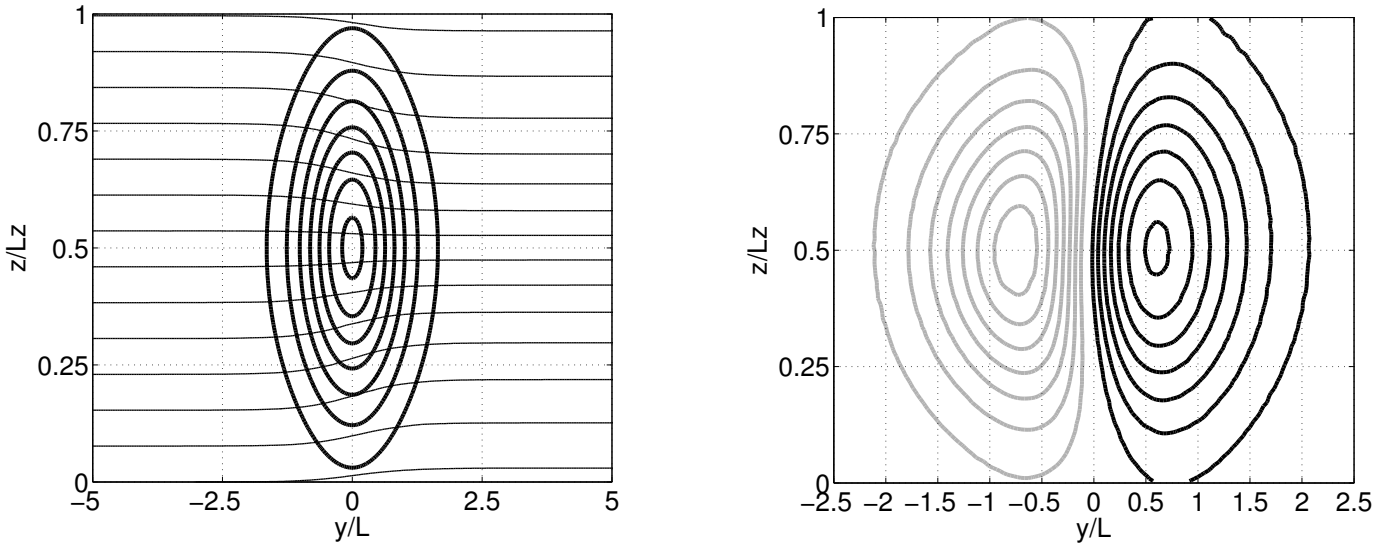

Initial jet for the *WRF* simulation. $Ro = 2$. $Bu = 1.9 \times 10^{-4}$.
Left: Temperature θ (thin black lines) and downstream velocity U (black lines). Contour interval $2K$ for θ and $2m/s$ for U.
Right: Vertical vorticity $\zeta = \partial_x v - \partial_y u$. Positive: *black*. Negative: *gray*. Contour interval $0.2 \times f$, starting from $0.2 \times f$.

Evolution of the along-jet Fourier modes

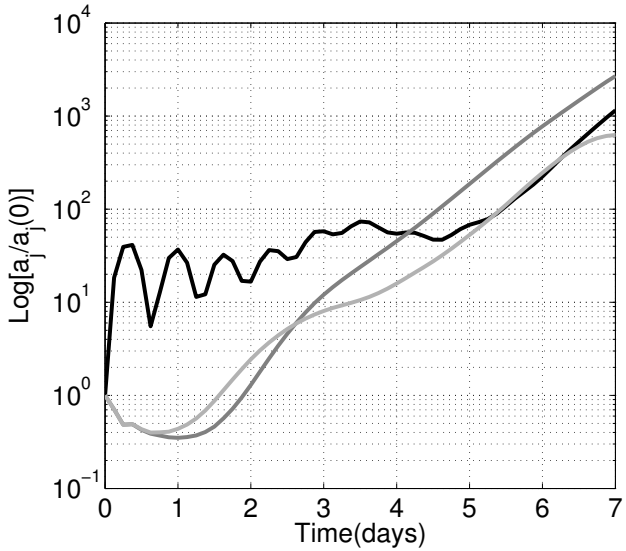

Evolution of the normalized kinetic energy of zero $< a_0 >$ (*black line*), first $< a_1 >$(*light gray line*) and second $< a_2 >$(*gray line*) modes of the along-jet Fourier transform.
$< a_0(t=0) > \approx < a_1(t=0) > \approx < a_2(t=0) >$.

Evolution of vorticity: across-flow view

day 0 at 00h00m00s

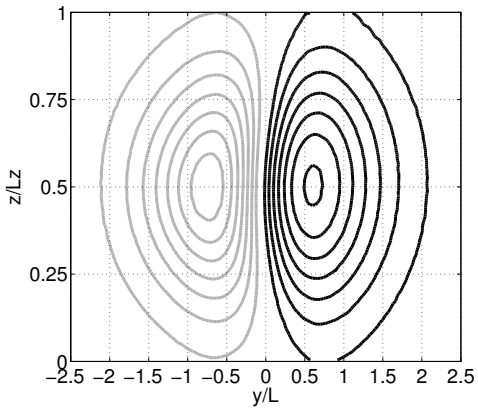

day 3 at 00h00m00s

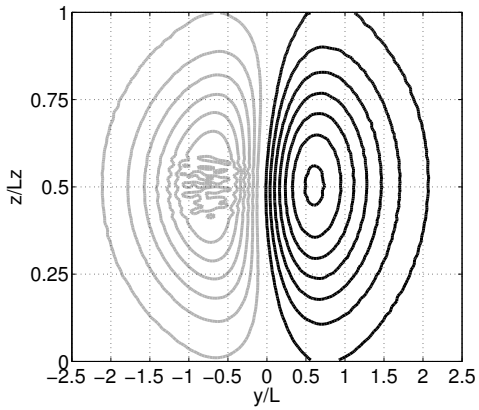

day 5 at 00h00m00s

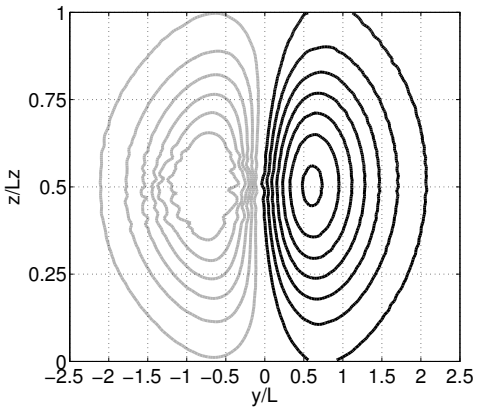

day 7 at 00h00m00s

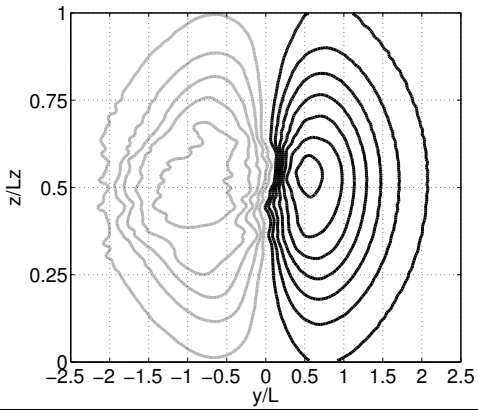

day 9 at 00h00m00s

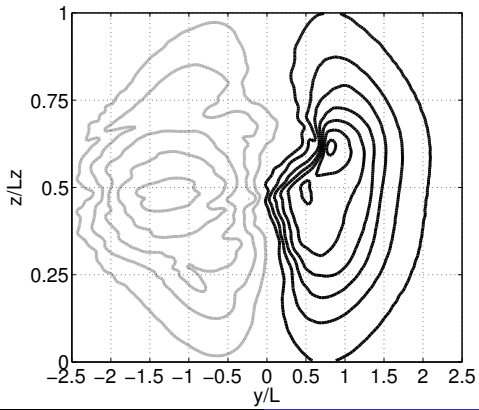

day 13 at 00h00m00s

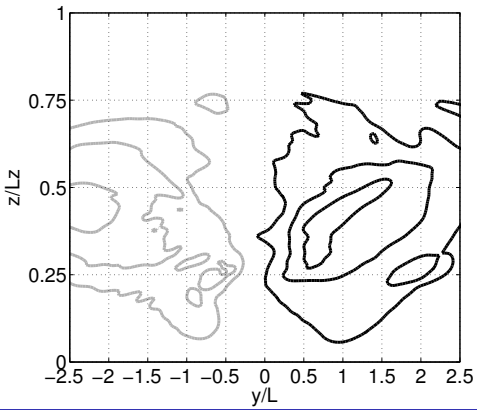

Evolution of vorticity: along-flow view

day 0 at 00h00m00s

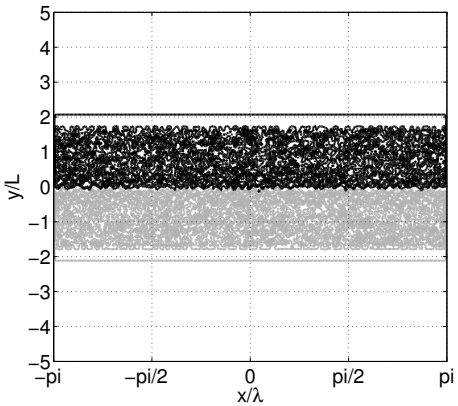

day 3 at 00h00m00s

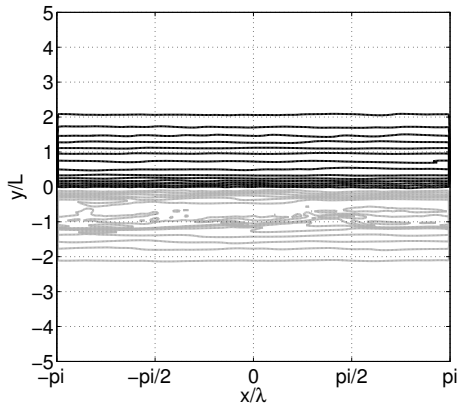

day 5 at 00h00m00s

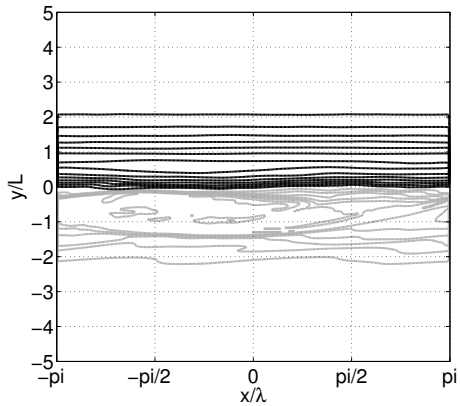

day 7 at 00h00m00s

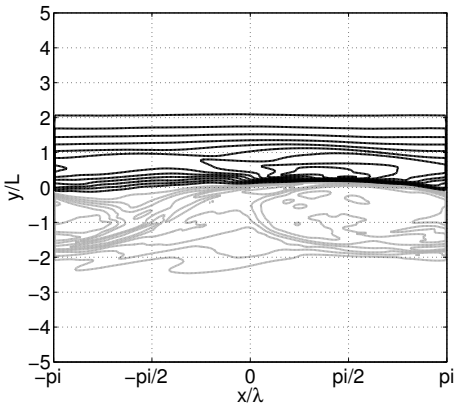

day 9 at 00h00m00s

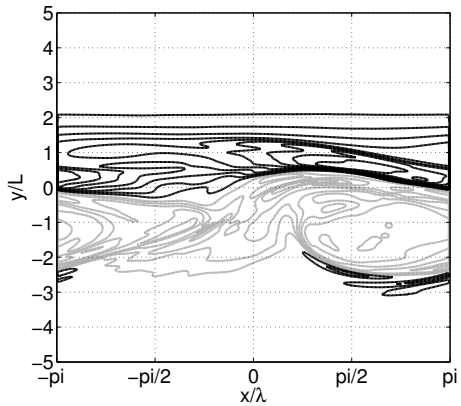

day 13 at 00h00m00s

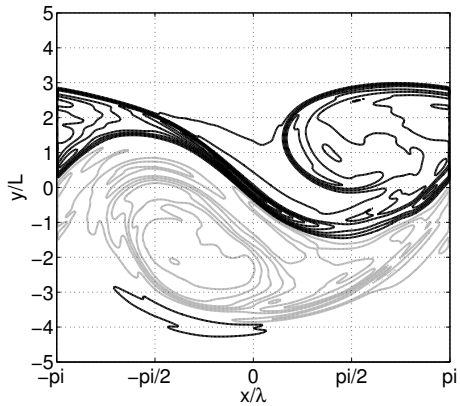

Summary of continuously stratified case, linear stability

- The leading instability of quasi-geostrophic jet is standard baroclinic (*B I*)
- The most unstable *B I* mode is cross-flow monopolar
- The leading long-wave instability of essentially ageostrophic jet is inertial (*I I*).
- A transition takes place at $Ro \approx 1.2$. *I I* coexists with standard *B I* then.
- In a wide range of (high) vertical wave numbers the asymmetric *I I* dominates
- At very high vertical wave numbers symmetric *I I* is the strongest.
- The most unstable *I I* mode is cross-flow dipolar,

Summary of continuously stratified case, nonlinear saturation

- *I I* rapidly develops from a small-amplitude white-noise perturbation
- Both symmetric and asymmetric *I I* patterns develop,
- Nonlinear saturation of *I I* produces homogenization of the cross-stream gradient of the vorticity in the unstable region
- At later stages *B I* takes over. Its saturation leads to formation of coherent vortices downstream.
- Persistent internal gravity wave emission accompanies the saturation process
- Vortex street formation results from the development of *B I* of the jet modified by the saturation of the inertial instability

Overall conclusions:

- *AII* dominant in a large range of vertical wavenumbers
- Saturates, like symmetric *II*, by massively producing overturning motions and enhanced dissipation and mixing
- Very high vertical wavenumbers needed to achieve the dominance of symmetric *II*
- *II* evolves simultaneously with /gives in to conventional barotropic instability

Remarks:

- Changing vertical resolution in essentially ageostrophic regimes may qualitatively change the output
- Similar program for centrifugal instability - similar results (Lahaye & Zeitlin, 2013).

References

- B. Ribstein, R. Plougonven and V. Zeitlin "Inertial, baroclinic and barotropic instabilities of the Bickley jet in two - layer rotating shallow water model", *Phys. Fluids, 2011*
- F. Bouchut, B. Ribstein and V. Zeitlin "Inertial vs baroclinic instability of the Bickley jet in continuously stratified rotating fluid" *J. Fluid Mech, 2013 - under consideration*
- B. Ribstein, A.-S. Tissier and V. Zeitlin "Barotropic, baroclinic, and inertial instabilities of the Gaussian jet on the equatorial β-plane in rotating shallow water model" *Phys. Fluids, 2013 - under consideration*